Distribution Agreement

In presenting this dissertation as a partial fulfillment of the requirements for an advanced degree from Emory University and its agents the non-exclusive license to archive, make accessible, and display my dissertation in whole or in part in all forms of media, now or hereafter known, including display on the world wide web. I understand that I may select some access restrictions as part of the online submission of this dissertation. I retain all ownership rights to the copyright of the dissertation. I also retain the right to use in future works (such as article or books) all or part of this dissertation.

Signature:

_____   _____

Dominic Robe   Date

Localized Dynamics in 2D Disordered Granular Systems

By

Dominic Robe

Doctor of Philosophy

Physics

Justin Clifford Burton, Ph.D.

Advisor

Stefan Boettcher, Ph.D.

Committee Member

Alessandro Veneziani, Ph.D.

Committee Member

Eric Weeks, Ph.D.

Committee Member

Peter Yunker, Ph.D.

Committee Member

Accepted:

Lisa A. Tedesco, Ph.D.

Dean of the James T. Laney School of Graduate Studies

Date

Localized Dynamics in 2D Disordered Granular Systems

By

Dominic Robe

Advisor: Justin Clifford Burton, Ph.D.

An abstract of

A dissertation submitted to the Faculty of the

James T. Laney School of Graduate Studies of Emory University

in partial fulfillment of the requirements for the degree of

Doctor of Philosophy

in Physics

Spring, 2019

Abstract

Localized Dynamics in 2D Disordered Granular Systems

By Dominic Robe

Disordered solids are ubiquitous in modern materials. The structural and dynamical properties of these materials are still poorly understood. Basic properties such as viscosity, elasticity, or magnetization can depend in a complex way on not just the elementary components of a material, but the details of its environment throughout its lifetime. In this thesis I describe and unify a set of phenomena in disordered systems which at first inspection appear anomalous and disconnected.

Physical aging is a relaxation process in which material properties appear to change over time despite fixed environmental conditions. This drift follows a sudden change in the environment to which the system could not equilibrate. Here I report analysis of experimental and simulation data which fit a trend in physical aging across a broad class of disordered systems. I implement particle tracking techniques and optimize simulations to observe dynamic trends over three orders of magnitude in time.

In dense disordered systems, movement of particles is generally intermittent and heterogeneous. I capture dynamical data with a fine enough temporal resolution to illustrate the obvious appearance of these sudden, localized rearrangements in a dense colloid. Paradoxically I also illustrate the lack of a distinction between a quiescent particle and one which is participating in a rearrangement. I resolve this conflict by measuring activity not by movement, but by contact with a neighboring particle.

The disordered structure in granular systems also leads to localized vibrational modes, which imbue systems with interesting acoustic and mechanical properties. I characterize the vibrational modes in systems of attractive particles with a variety of disorder types. Some acoustic properties are attributed to quantum mechanical effects. I demonstrate that similar effects can be present in a classical system.

All the phenomena I report here speak to the complexity of behavior that arises from a rough energy landscape. Localization, intermittency, history-dependence, and decelerating relaxation can all be found in a system with simple interactions if the multitude of interactions become frustrated. This critical feature connects the dynamics of disordered granular systems intimately with a vast field of complex systems.

Localized Dynamics in 2D Disordered Granular Systems

By

Dominic Robe

B.S., Tennessee Tech University, Tennessee, 2014

Advisor: Justin Clifford Burton, Ph.D.

A dissertation submitted to the Faculty of the
James T. Laney School of Graduate Studies of Emory University
in partial fulfillment of the requirements for the degree of
Doctor of Philosophy
in Physics

Spring, 2019

Contents

List of Figures

Citations to Previously Published Work

Chapter 2 contains research from the following publication:

- *"Record Dynamics: Direct Experimental Evidence from Jammed Colloids"*, **Dominic Robe**, Stefan Boettcher, Paolo Sibani, Peter Yunker, *Europhysics Letters*, **116 (3)**, 38003, (2016)

Chapter 3 contains research from the following publication:

- *"Two-time correlations for probing the aging dynamics of glassy colloids"*, **Dominic Robe**, Stefan Boettcher, *Soft Matter*, **14 (46)**, 9451-9456 (2018)

Chapter 4 contains research from the following paper:

- *"Aging is a log-Poisson process, not a renewal process"*, Stefan Boettcher, **Dominic Robe**, Paolo Sibani, *Physical Review E*, **98 (2)**, 020602 (2018)

Acknowledgments

With the submission of this thesis, I would like to acknowledge those who have made my journey toward this achievement not only possible, but enjoyable. I thank Professors Stefan Boettcher and Justin Burton, my advisors, for providing me with encouragement and advice throughout my time here. If not for their willingness to collaborate and help me pursue my ideas this would have been an arduous journey. I thank Stefan for encouragement to make connections with people. I thank Justin for creating a jovial workplace.

I thank Professors Eric Weeks and Connie Roth for extensive discussions about the assortment of topics in soft condensed matter and for their patient reminders of the differences between reality and computer code. I thank the members of my thesis committee for feedback to improve my work. I thank the faculty of the departments of Physics and Computer Science for providing rigorous and stimulating lectures, and for cooperating to provide me the opportunity to pursue this interdisciplinary work. I thank my high school astronomy professor, Mr. Rutherford for getting me hooked on research. I thank my professors from undergrad, particularly Dr. John Shriner for encouragement to explore the world of research.

I want to thank my cohort, Guga, Mike, Nicholas, Jennifer, Benjamin, Xiaolei, Yannic, Robert, CC, Joe, Ahmed, and Stephen for all their friendship and discussions.

Finally, I want to thank my family for encouragement and support to pursue my interests, contribute to the world, and enjoy life.

Dominic Robe

Emory University, Atlanta, USA

Spring 2019

Dedicated to my parents

Gary and Corlis

with gratitude.

Chapter 1

Introduction

1.1 Glass

1.1.1 Disorder

In elementary school, one learns about crystalline solids and amorphous liquids. Reality is moderately more interesting. The vast majority of solid materials in modern applications are disorganized at the microscopic level. Materials colloquially known as 'glass'[1], 'rubber'[2–4], 'plastic'[5, 6], some ceramics[7], biological systems [8–10], and foodstuffs [11, 12] don't have a crystalline structure. The properties of these materials can be explained once they are discovered, but there is no way presently to predict the properties of a material directly from its components. Even that unsolved problem would be secondary to the goal of starting from a desired property and designing a material to fit that need.

If one has a material composed of a multitude of identical particles, be those

atoms or grains of sand, the material properties are determined by two things. One is the properties of the individual particles, and one is their arrangement. A block of gold has different properties than a block of lead. They have the same crystal structure, but the atoms are different. A block of graphite is different than a block of diamond. They have the same atoms, but a different structure. The repetitive nature of crystalline materials allows us to consider one tiny unit and calculate the properties of an infinite repetition of that unit. Physicists and Chemists and Engineers have had great successes with this method for a century.

In a disordered solid there is no repeating unit, so at first glance one would have to consider the influence of every single particle to understand the system. Since there are billions upon billions of molecules in even the tiniest object, computing all the interactions is impossible. So, one runs simulations of thousands or millions of particles, and compares the results to experiments on useful volumes of real materials. Scientists have had increasing success with this method over the last few decades.

The particles which make up a disordered solid may be atoms, small molecules like SiO_2 (window glass), large molecules like polyethylene (plastic), grains [13–18] like in concrete, bubbles [19–21] like in Styrofoam, or even active particles like cars in a traffic jam [9, 22, 23]. In this thesis, the term 'glass' refers to any sort of disordered system which appears to be solid.

So, what are the properties of glasses that are so interesting? The most intuitive property is viscosity, or resistance to flow. One generally assumes that solids have infinite viscosity. This can't be strictly true, since metal can be shaped. What is true is that classical materials have a discontinuous change in viscosity as they

freeze. Glasses, on the other hand, become progressively stiffer as they vitrify [24]. This change can be remarkably sudden to human perception, but there is no discrete change in the viscosity. In fact, even after a glass appears to become solid, it has a measurable viscosity, which continues to increase as the material is cooled.

It should be clarified what is meant by 'cooled'. In grade school, one is taught that temperature determines if something is liquid or solid. Later, one learns that pressure also matters. It is also known that if a system is being stirred up, this can also affect freezing. In some systems, the application of a magnetic field is also important [25, 26]. In polymer solutions [27], colloidal suspensions [28–30], and granular media [31–33], the concentration is key. In general, each of these parameters can be defined in such a way that zero is more likely to be solid and higher numbers are more likely to be fluid [34]. The reader should be aware that many of the phenomena which appear 'as a system is cooled' have analogs as a system is compressed or as some other control parameter is changed. Similarly 'to quench' literally means to cool rapidly, but here can mean to change any environmental condition rapidly to the glassy regime. A material which can become a glass under some set of conditions is here called a 'glass former'.

So as a glass former is quenched, it vitrifies (forms a glass) and viscosity increases dramatically. The temperature at which the material seems to a human to be a solid is defined as its glass transition temperature T_g. In glassy materials this resistance can also depend on the speed of the flow. If one squeezes a ball of putty, the flow is slow, and the putty deforms. If one throws the putty, the putty's collision with the floor is fast, and the putty resists the flow and bounces (shear thickening). Note

that window glass is an extreme case several hundred degrees below its T_g at room temperature, which makes it extremely solid. In most of this thesis I will concentrate on glasses very close to the glass transition, which behave more like chocolate: capable of brittle or viscous deformation, and very sensitive to temperature.

The combination of temperature and flow speed can interact in a variety of ways to produce interesting and useful functions. Some polymer solutions have decreased viscosity in fast flow (shear thinning), so are introduced to oil pipelines to speed up transportation [35, 36]. Medical problems sometimes call for artificial replacement of tissues such as joints or skin. For these replacements to be functional they must closely mimic the elastic properties of the original tissue [37, 38]. Soil liquefaction is a phenomenon in which vibrations or surges of ground water reduce the stiffness of soil, which can cause whole buildings to fall [39, 40]. Common plastics are popular because they are solid at room temperature, but moldable at easily accessible temperatures. Better understanding of the general principles of disordered materials improves performance in all these situations.

Viscosity is not the only interesting property of glasses, either. Light propagates differently through a disordered medium, which makes the transmission and index of refraction depend dramatically on the wavelength of light [41, 42]. The highly porous nature of disordered materials makes them useful for filtration [43–45]. The complex topology of these systems also affects their thermal [46, 47] and electrical conductivity [48–52]. Finally, the assortment of vibrational modes give glasses interesting acoustic properties [53–59] and a different heat capacity than in crystals [47]. These are just some of the well-documented properties that are still being explored in disordered

solids.

1.1.2 Frustration and satisfaction

The commonality between the assortment of systems that present these surprising properties is not only disorder, but frustration. When there are multiple constraints on a system, which cannot all be mutually satisfied, the system is called 'frustrated' [60]. If there are a multitude of particles, each trying to optimize its own position, they all get in each other's way, and none can fully organize themselves [61]. Such a system quickly finds a stable but extremely delicate configuration. A cup full of sand is mechanically stable, but the slightest tap will see the sand compact as the grains reorganize themselves [62–64]. This sensitivity (called marginal stability[34, 65, 66]) gives glasses their interesting plastic and elastic properties, depending on the vigor with which they are perturbed. Meanwhile, the vast assortment of configurational possibilities complicates prediction of these properties.

Frustration can be interpreted as a constraint satisfaction [67] or optimization [68, 69] problem. Particle positions are variables and interaction potentials and environmental conditions are constraints. As environmental conditions change, the number of satisfactory configurations shrinks rapidly. Eventually the space of solutions can become disjointed, locking a system into a particular configuration. To be precise, a system is only 'frustrated' if there is no configuration that satisfies all of the constraints [60], as in Figure 1.1. Colloquially the term can apply to systems which have a solution, but it can't be reached without temporarily violating more constraints (sometimes called geometric, topological, or structural frustration)[70, 71].
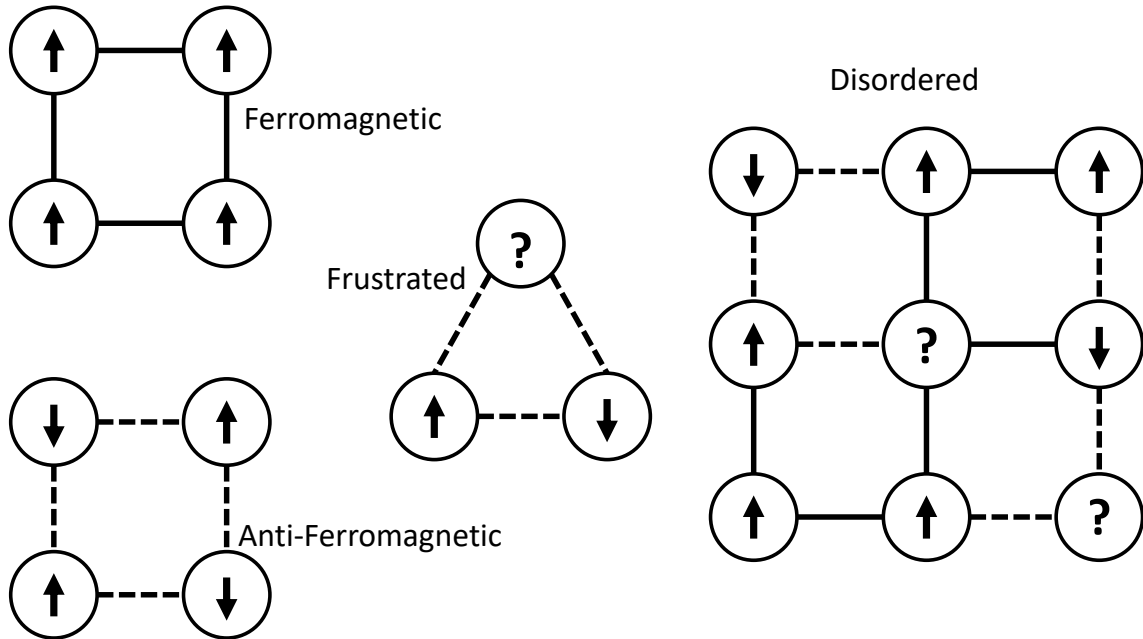
Figure 1.1: Diagram of spin glass features. Ferromagnetic (solid) bonds favor aligned spins, while anti-ferromagnetic (dashed) bonds favor opposite spins on either end. Anti-ferromagnetic bonds on a triangular lattice are always frustrated, meaning there is no solution which satisfies all bonds, even though the bonds are not disordered. A system with disordered bonds may have a totally satisfied state, but finding it is difficult, especially if the system is trapped in a locally optimal state.

For instance, a packing of spheres may be most dense as a crystal, but a crystal can't always be formed from a dense disordered packing without spheres interpenetrating.

1.1.3   Spin glass

The simplest case of constraint satisfaction is the Boolean satisfiability problem 'SAT', which was the first problem proven to be NP-complete [72]. A related physical system is a 'spin glass' [61, 73]. A spin glass is a system of objects (spins) which can occupy either the 'up' or 'down' state, as in Figure 1.1. Each pair of spins has either a 'ferromagnetic' bond which makes them prefer to be in the same state or an

'anti-ferromagnetic' bond which makes them prefer the opposite state. These bonds are equivalent to the Boolean expressions 'a AND b', or 'a AND NOT b' respectively.

Spin glasses are experimentally realized in a number of ways [74], the archetype of which is a noble metal such as gold doped with a few percent of magnetic ions, such as iron [75–77]. Indirect interactions between the magnetic moments (spins) of the dilute ions produces an effective interaction potential that oscillates over long distances, so some ions interact positively and some negatively.

Spin glasses have been successfully modeled for decades [73, 78–83] using binary spins and random interaction energies drawn from a Gaussian distribution with zero mean and unit variance. Often the interactions are simply ± 1. Systems are simulated using the Metropolis algorithm [84, 85]. In short, this is a Markov chain Monte Carlo algorithm in which for simulation time step, each spin attempts to flip. If the flip would decrease the potential energy, it is carried out. If the flip would increase the potential energy by ΔE, it is carried out with probability

$$P = e^{-\Delta E/T}, \tag{1.1}$$

where T is the simulation temperature in units such that the Boltzmann constant is 1. The Metropolis algorithm satisfies detailed balance, so states are sampled in their equilibrium distribution if the system is simulated long enough.

When a spin glass is held at high temperature, there is energy to spare, and each spin can fluctuate between the two states. At zero temperature, though, the probability in Eqn. 1.1 is zero, and no spin can flip if that flip would increase its potential energy. This means the system gets trapped in a local energy minimum,

even though a more optimal configuration may exist. At intermediate temperatures, spins have a finite probability of flipping into a worse configuration, which might cross an activation energy barrier to a more optimal configuration. A sequence of these activated relaxation events gives rise to a process called physical aging [76, 78, 86–88].

1.2 Aging

1.2.1 Slowing down

Humans intuitively recognize that materials change over time. Ice melts, metal rusts, leaves decay, plastics become brittle. All of these represent some equilibration between the material and the environment. Ice reaches thermal equilibrium with the air. Microbes spread out the energy stored in plant matter. Materials may absorb oxygen out of the atmosphere. All these processes will eventually reach equilibrium with the environment and halt.

In a frustrated system, equilibration can take a very long time. Since there is no manager telling each piece of a system where to go, the first stable position that a system comes to is likely not the lowest possible energy. A configuration that is mechanically stable but not the absolute lowest energy state is called metastable. Fluctuations such as thermal motion or vibrational noise can easily knock the system out of this metastable state, allowing it to look for a better one. Since each new stable state is marginally better than the last, it will take longer for fluctuations to drive the system over the activation barrier to the next state. This process causes the equilibration of a glass to slow down over time.

It should be noted that humans also intuitively recognize that equilibration slows down over time. A very hot cup of coffee cools rapidly at first, but will remain lukewarm for much longer. The temperature difference between two systems in fact decays exponentially as

$$\Delta T = \Delta T_0 e^{\frac{-t}{\tau}}, \tag{1.2}$$

where τ is the time scale of the relaxation. This exponential decay is present in all classical equilibration processes. Relaxation in a glass, however, is an even more drawn out process which is known as 'physical aging', or just 'aging'. This process is 'frustration limited' as opposed to the regular 'gradient limited' equilibration.

One example of this slow relaxation is the density of a polymer glass [89]. The density of a fluid generally increases with colder temperatures. If one cools a polymer melt quickly, it vitrifies and cannot reach its more compact equilibrium density. One can then measure the thickness of a polymer glass film as a function of time. If one tried to extract a value of τ from this data set, the apparent value would increase the longer the experiment is run. For this reason, relaxation in glasses is often described as 'extremely slow', or with a 'growing time scale'.

To be precise, though, physical aging is qualitatively distinct from regular equilibrium relaxations. The volume relaxation, for instance, appears to follow the form

$$\Delta V = \Delta V_0 - \beta \log(\frac{t}{\tau}), \tag{1.3}$$

where β is the 'aging rate' [89]. Clearly this trend cannot continue indefinitely, since $\beta \log(\frac{t}{\tau})$ will eventually become larger than the initial excess volume ΔV_0. Due

to the logarithmic dependence on age, this crossover can occur on geological time scales, and the system is considered permanently out of equilibrium.

In practice, if a material's glass transition temperature is near its operating temperature, it ages only briefly, but its properties can change dramatically with changes in temperature, as discussed in Section 1.1.1. If a material is used in an environment hundreds of degrees below T_g, then aging can be so slow as to not practically affect its properties. Recent experiments on 20-million-year-old amber found it to be not yet fully equilibrated [90]. There is an intermediate regime where physical properties of materials can change over a course of months or years, which is harmful to many applications.

Filtration systems make use of glassy polymers precisely because of their porous structure. As that polymer ages, its constituent molecules find a more efficient packing structure, and the filter becomes less permeable [91]. Polymer films also find usage as dielectric layers in capacitors. As the film ages, its dielectric constant changes, affecting the behavior of the capacitor [92]. Without an understanding of physical aging, knowing what to expect from a material in a couple of years requires waiting a couple of years to see what happens to test samples. This strategy is not fast, good, or cheap.

1.2.2 Over the hill

A picture that is often described is that of an 'energy landscape' [93–95], with high energy peaks, low energy valleys, and saddle points marking the easiest path from one minimum to another. Aging is then the process of climbing through successive moun-

tain passes, seeking the lowest lying valley. This picture assumes a two-dimensional, continuous configuration space. In a system of repulsive particles, the potential energy depends on the position of all N particles, making the 'landscape' $3N$-dimensional. However, there are still local minima, metastable states which would increase in potential energy if any particle moved, and there are still critical points which form the easiest route through configuration space.

We can then consider the number of valleys of a particular depth, and the heights of the saddle points connecting them [84, 96–98]. Equilibrium statistical physics teaches us that the chance of crossing such a barrier decays exponentially with its height, and increases exponentially with temperature, as in Eqn. 1.1. If a system crosses into a lower valley, dissipating free energy, it will be exponentially harder to cross back via the same route. Such a reconfiguration is therefore referred to as 'irreversible'. This irreversibility is amplified by the fact that in a high dimensional configuration space, there are a vast number of other directions the system could move, making a re-traversal of the same path unlikely. So the progressively more difficult process of escaping from deeper minima makes aging a very slow and ever-decelerating process. Yet the profuse number of minima in a high dimensional complex landscape mean that there is always a lower energy configuration somewhere, so physical aging never really stops.

In a spin glass, introduced in Section 1.1.3, one can easily consider the heights of these hills and valleys quantitatively [99]. Recall from Section 1.1.2 as well that this binary model represents a broad class of frustrated systems. Consider particularly the case where all interactions between spins are ± 1, so a particular spin's contribution to

the system's potential energy is simply the number of its bonds which are unsatisfied. If that number is more than half its bonds, the spin will immediately flip. If the number is less than half, the spin has a probability of flipping which decays exponentially with the number of satisfied bonds, as per Eqn 1.1. If just one spin flips to a higher energy state, it will flip back in the next simulation step, so crossing a barrier to a different stable state requires waiting for multiple spins to flip simultaneously. This brings us to the important topic of cooperation.

1.3 Cooperation

One of the hallmark features of glassy systems is dynamical heterogeneity. Most components of a system spend most of the time in one fixed location or state. Occasionally, a small region of the system will become active. A cluster of particles may shift slightly in a colloid or granular packing. A set of spins may flip. A section of polymer chain reconfigures itself. This localized region of dynamically active particles may be called a cooperatively rearranging region (CRR) [100–106], a thermally activated event [84, 107–109], or an irreversible rearrangement [30, 110, 111]. These events are distinguished from reversible fluctuations of a single particle's position as it rattles around between its neighbors. A particle may move from one side of this cage to the other and back, but if the whole cage moves, going back is impossible.

These rearrangements are generally rare and short-lived. Near the glass transition, constraints between particles are tight, so dozens of particles may need to coincidentally move in the same direction to permit a rearrangement. The relevant unit of time becomes how long it takes a particle to cross from one side of its cage

to the other, t_{cross} (which can be on the order of picoseconds for molecular systems, or milliseconds for colloidal particles). A single particle may participate in an event as rarely as once in hundreds or thousands of t_{cross}, even in the supercooled regime. Beyond the glass transition these events become rarer with time as a system ages, as discussed in Chapter 4. In contrast, the actual duration of an event is generally just a few t_{cross}, so capturing fully the dynamics of a glassy system requires capturing and processing data over several orders of magnitude in time.

The motion of an individual particle is usually a random walk through its cage. As such, motion of adjacent particles is generally uncorrelated. Therefore, the probability of two particles moving in the same direction is the joint probability of each particle moving that way on its own. The chance of a cluster of n particles moving in a coordinated way by sheer coincidence is then exponentially small in n. This vanishing probability creates a barrier to rearrangement even in the absence of potential energy and thermal fluctuations. Such a barrier is referred to as an 'entropic' barrier [112] as opposed to an energetic one.

The appearance of this intermittent, heterogeneous behavior would suggest the existence of two populations of particles: active ones and caged ones. Particles may momentarily enter the active population, then settle in a new cage. Distinguishing when a particle is or is not rearranging turns out to be a challenging problem. The typical strategy is to consider the 10% of particles with the largest displacements [30, 113–115]. However, the change in position due to a rearrangement can be much less than the size of a cage, so not all of the 'fast' particles are rearranging and not all of the rearranging particles are fast [116]. Our solution to this problem involves

detecting when a particle encounters a new neighbor, which will be discussed in Chapter 3.

1.4   Soft Spots

The structural disorder discussed in Section 1.1.1 and the dynamical heterogeneity discussed in Section 1.3 would seem to suggest the presence of some structural heterogeneity. There could be regions of a system which are structurally predisposed to rearrangement, while other regions are particularly stable and organized. In this section we describe two perspectives for analyzing structural properties of disordered solids.

1.4.1   Local order

If disorder is the source of interesting behavior in glasses, perhaps a measure which picks out regions of well-organized particles would be useful. The most common measure of local order is the Bond-Orientation Order (BOO) parameter [117–119], denoted by ψ_6 in 2D. The 'orderedness' of particle j is then

$$\psi_{6,j} = \sum_{k=1}^{z_j} e^{i6\theta_{jk}}, \tag{1.4}$$

where z_j is particle j's coordination number (number of adjacent particles), and θ_{jk} is the angle from the x-axis to the line between particles j and k. If all of j's neighbors are arranged in a perfect hexagon, then ψ_6 is 1. If j has 5 or 7 neighbors and they are not evenly spaced, values of ψ_6 tend to be around $\frac{1}{2}$, with configurations closer to

a hexagonal lattice having higher values.

Two questions are then obvious. What correlation is there between microscopic dynamical heterogeneity and local structural order? Is the dramatic increase in viscosity across the glass transition due to the presence of ordered regions? The answers to both questions are yes and no. Less ordered regions are more likely to rearrange [119], but they are not guaranteed to do so. The system averaged orientational order does increase as the glass transition is crossed [30, 120], but not by nearly enough to produce the observed phenomena.

There is a similar metric which measures icosahedral order in 3D [121, 122]. There are also more sophisticated metrics, culminating with machine learning algorithms which consider the positions of dozens of particles [123–126]. These methods can achieve high correlation with the likelihood of a particle to participate in a rearrangement. However, since these many-body systems are highly chaotic, no measurement of just positions can predict exactly when and where dynamical events will occur.

Simulations provide a unique opportunity to study the probability of particular regions to rearrange, and the effects of those events on nearby structures. A simulation can be reset to a configuration from before an event, then the particle velocities may be randomized and the simulation run again. By repeating this protocol, one can count the fraction of simulations in which a particle participates in a rearrangement [127]. One can also measure the distance between copies of a particle with different dynamical histories.

Aside from the effect of structure on dynamics, one can also investigate the effect of active events on structure. In general, rearrangement events tend to increase the

structural order in their vicinity [30, 123]. This makes further rearrangements in the same area less likely. Sometimes, as the surrounding system responds to a new local structure, some distant areas can marginally reduce their degree of order. But as a system ages, the ordering of the system overall increases.

1.4.2 Vibrational modes

A 'normal mode' of a many-particle system is a pattern of motion in which all of the particles oscillate sinusoidally with the same frequency. These modes are called 'normal' because they are orthogonal and therefore linearly independent. Practically this means if a system is oscillating in a normal mode, it will continue to oscillate in that mode at a particular frequency indefinitely. Any vibrational motion of a system can then be decomposed into a linear combination of normal modes, which may evolve over time.

If a glassy system is trapped in a local energy minimum, as discussed in Section 1.2.2, one can extract vibrational properties from the potential energy near that minimum [33, 65, 128, 129]. As long as the system doesn't undergo a rearrangement, the motion of particles in their cages can be described as vibrations around the minimum. Derivatives of the system potential energy with respect to the particle positions provides information about the normal modes of the system. This calculation is discussed more thoroughly in Chapter 5.

In a homogenous, ordered system the normal modes are generally plane waves, but in a disordered system they can have remarkable structure. Particles which happen to be less tightly constrained will oscillate at particularly low frequencies, creating

'localized modes', where just a few particles really participate in the oscillation [128, 130–132]. These localized, low frequency modes are a pathway to rearrangement, creating another link between disordered structure and heterogeneous dynamics.

The peculiar spectrum of vibrational modes in glasses is intimately linked to some of their stranger properties. At very low temperatures (less than 1 Kelvin), glasses exhibit a number of interesting acoustic behaviors. They may attenuate certain frequencies of sound, until the amplitude of that sound becomes too high, at which point it propagates normally (known as saturation of attenuation) [53, 59]. If a glass is excited by two acoustic pulses separated by time t, the excitations quickly decay, but at time $2t$ the system apparently re-excites itself (known as a phonon echo) [59, 133]. The most recognized theory to date to explain these phenomena fails to explain several experimental details, which will be discussed in Chapter 5.

1.5 Thesis layout

In this chapter I have laid out the surprising phenomena observed in disordered solids in a manner to best introduce the progress reported in this thesis. The rest of this thesis is organized as follows.

In Chapter 2 I describe analysis of data from an experimental two-dimensional colloidal suspension undergoing physical aging. I will introduce the theoretical framework of 'record dynamics' and use it to describe the time-dependent activity in the data. I will also compare these results with a coarse-grain numerical model based on record dynamics.

In Chapter 3 I describe a series of particle dynamics simulations carried out to

emulate and expand upon the experimental data in Chapter 2. I discuss an algorithm based on Voronoi tessellation which distinguishes between caged and rearranging particles. I also show that the distribution of particle displacements depends on both the time scale for displacement and the age of the system. I show that this detailed measurement simplifies dramatically in the reference frame of record dynamics.

In Chapter 4 I describe the statistics of cooperative event rates from my particle dynamics simulations and spin glass simulations. I compare these statistics to the record dynamics prediction and to the prediction of a competing model.

In Chapter 5 I describe particle dynamics simulations of oscillating masses interconnected by a network of anharmonic springs. I introduce disorder to the system and describe the effects of this on the vibrational modes of the system. I develop a protocol by which an externally applied plane wave pulse can couple with a localized vibrational mode and deposit energy there. I discuss the implications of this phenomena for low temperature glasses.

In Chapter 6 I discuss details of the computational methods employed in the development of this work. I describe prevalent methods used in studies similar to mine and the motivations for my choices of methods and parameters. I also describe my modifications to some algorithms for my specific purposes.

In Chapter 7 I discuss the generality of these findings for the variety of disordered solids and complex frustrated systems and make some concluding remarks.

Chapter 2

Aging in a 2D colloidal suspension

2.1 Introduction

Aging is a decelerating process present in manifold complex materials relaxing after a quench. It has been studied for decades from different perspectives [30, 76, 80, 87, 110, 134–150], with the experimental focus moving, over the years, from relations such as the Fluctuation-Dissipation theorem and its violation [134, 135] on to the discovery, observation and study of the 'anomalous' non-equilibrium events [30, 80, 110, 136–138] now recognized as key properties. Concomitantly, theoretical and numerical studies have also considered anomalous events [87, 139, 140], and spin-glass thermo-remnant magnetization [141], magnetic flux creep in type-II high-T_c superconductors [142], ants moving out of their nest [145] and particle motion in dense colloids [148–150] have been interpreted using the statistics of 'quakes'. These increasingly rare cooperative changes are spatially localized within domains or clusters and lead the system from one metastable state to the next. The coarse-graining scheme referred

to as 'record dynamics', links quakes with crossings of record high peaks in the free energy landscape [151, 152] associated to growing clusters and generated by the well-known exponential proliferation of local minima ('inherent states') with growing energy [153, 154]. In dense colloidal suspensions, quakes are usually called 'cage breakings' while reversible quasi-equilibrium (or Gaussian) fluctuations are called 'cage rattlings' [30, 113, 155].

Record dynamics has been proposed as a tool to model complex systems [152, 156] based on its ability to explain in a unified fashion the phenomenology of many different aging systems by filtering away all their microscopic peculiarities. The concurring experimental evidence pertains to macroscopic properties of magnetic glasses [139–141] and dense colloidal suspensions [148, 149]. However, direct experimental support of its basic microscopic assumption is hard to gain and has been unavailable so far.

The data analyzed here stem from three experimental runs by Yunker et al [30] who employed an aqueous bi-disperse suspension of micro-gel spheres sandwiched between glass cover slips to form a quasi-2D colloidal system with the unique property that a temperature change of $\approx$ 4K at room temperature, could change the area fraction by $\approx$ 10% in $\approx$ 0.1s. The systems were prepared at a high packing fraction, heated uniformly by a mercury lamp to form a colloidal fluid, then quenched to form a glass by removing the light. Final area fractions studied were in the range 81-84%. (the glass transition in 2D granular systems is 82% packing fraction). A window of 2,500 particles, embedded in a sea of 300,000, was then tracked for 10^4s. Most of the data presented here and in Ref. [30] stem from samples at the highest packing fractions and exhibit the strongest aging behavior, while our analysis of the
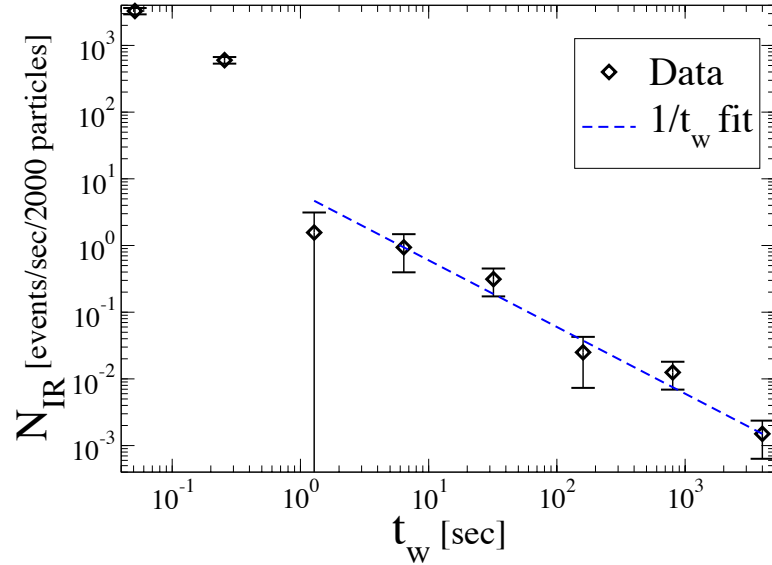
Figure 2.1: Decay in the rate of intermittent cage-breaks ("quakes") in a dense colloid. Re-plot on log-scale of the experimental data in Fig. 2a of Yunker et al. [30]. The data directly satisfies the $1/t$-decay fundamental to record dynamics that justifies the log-Poisson statistics [149, 150].

loosest packings shows deviations from it. In Ref. [30], dynamic heterogeneity and aging were studied through analysis of changing particle neighborhoods. Here we use a threshold of $0.4\mu m$ to separate small reversible in-cage motion from irreversible displacements. Importantly, once irreversible configurational changes are identified, the significance of rare individual cage breaks for intermittency is demonstrated, and the connection between small and seemingly insignificant localized dislocations and much larger collective shifts in particle position is established.

These experiments provide the first opportunity to confront both the central assumption of record dynamics on quake statistics, as shown in Fig. 2.1, and one of its predictions, namely the emergence of growing mesoscopic real-space structures. In this chapter, we analyze the data of Ref. [30] to show that they concur with the

fundamental assumptions as well as with the predictions of the theory. For the first time, direct experimental evidence for record dynamics as a coarse-grained description of dense colloids in particular, and of a broad class of aging materials in general, is provided.

2.2 Theoretical background

The relevance of records is immediate in the "Backgammon model" [157], in which m particles are distributed over n boxes ($m \gg n \gg 1$) and where each update swaps one particle randomly between boxes. A box which empties out by a chance fluctuation of size $\sim m/n$ becomes inaccessible as the system's energy corresponds to the number of occupied boxes. The dynamics thus requires a sequence of *rare* record fluctuations of *marginally* increasing average size $\sim m/n, \sim m/(n-1), \sim m/(n-2), \ldots$, to progress ever more slowly towards its ground state where all particles fit into *one* box. The importance of intermittent, irreversible record-events that are decorrelated by an exponential separation of time-scales is obvious. Finally, the connection between decelerating dynamics and growing mesoscopic real-space objects, our clusters or domains, is studied theoretically in Ref. [158], using a simple kinetically constrained model, the "parking lot model" [159], which has been applied in Ref. [64] to explain the logarithmically slow compactification of granular piles.

In disordered systems with a large number of degrees of freedom, the concept of "marginal attractor stability" first introduced in [160] is of central importance. In our context it presupposes three features that are well-established for the coarse-grained free energy landscapes of complex systems, as illustrated in Fig. 2.2: (1) Meta-stable

states with their combined basin of attraction, proliferate exponentially for increasing free energy [153, 154, 161, 162]; (2) More-stable (lower-energy) states typically have higher barriers to escape their basin [162, 163]; and (3) overcoming increasingly higher barriers makes exponentially more configurations accessible [164]. The ensuing dynamics is also illustrated in Fig. 2.2: In a quench, the system almost certainly gets stuck initially in a shallow basin of high energy. There, a small, random fluctuation already suffices to escape into a larger basin containing many sub-basins, some of which feature local minima of lower energy. But for basins of lower energy, gradually higher fluctuations are required to escape. The gain in stability acquired in any one of these escapes will most probably only be *marginal*, since spontaneously arriving at minima of dramatically lower energy would be exponentially unlikely. In such a marginally deeper basin, the motion in and out of states less stable than the original basin only provides reversible quasi-equilibrium fluctuations. For an irreversible quake, typically, merely a record fluctuation in the random noise impinging on the system is required [165]. In a spin glass a record-high thermal energy fluctuation elicits a quake associated with a large decrease in energy [87]. In a colloidal glass, record-sized fluctuations of locally available free space are needed to accommodate a new particle, and the final effect of a quake is a density increase.

In this manner, on exponentially longer timescales, ever larger and rare fluctuations become possible such that incrementally higher barriers can be scaled in a sequence of intermittent record-sized events, thereby making an exponentially growing number of configurations accessible. This approximation supersedes the particular properties of the hierarchies of barriers in a given system. As long as such a hierarchy
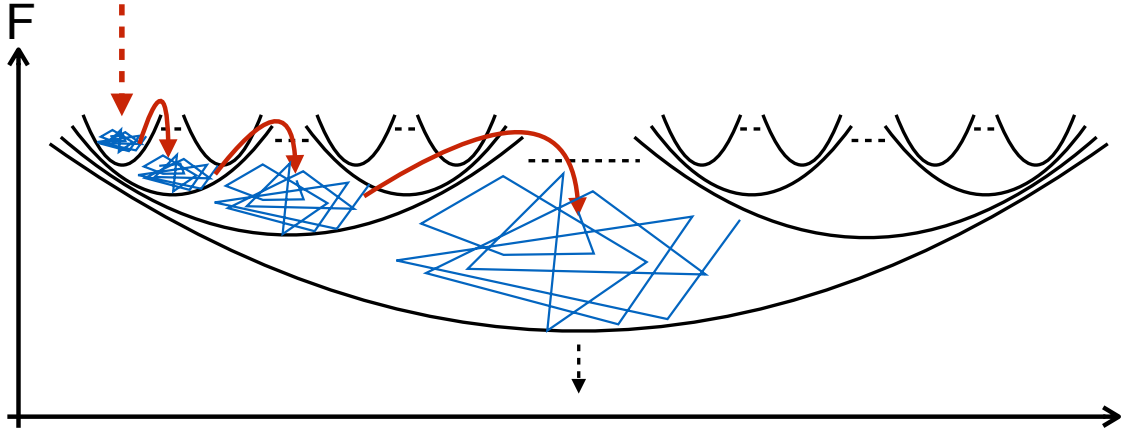
Figure 2.2: Schematic view of the hierarchical free-energy landscape of a small jammed system (solid black), with a typical trajectory of an aging dynamics (blue and red). With increasing free energy F, local minima proliferate exponentially but also become shallower. The black-dashed down-arrow signifies that the hierarchy continues to a distant ground state. The dynamics generically evolves after a quench (red dashed arrow) through a sequence of quasi-equilibrium explorations (blue trajectories) and rare, intermittent quakes over record barriers (red arrows) that access an exponentially expanding portion of the configuration space.

exists, i.e., the system is actually jammed, these differences only vary the overall unit of time. To summarize, if barrier heights only grow marginally from one quake to the next, quake statistics can be meaningfully approximated by the statistics of record sized fluctuations in the random white noise which drives the dynamics [165]. Record dynamics thereby offers an analytical in-road to coarse-grained descriptions able to straddle the aging phenomenology. The experimental data presented here are compared to the 'cluster model' [150], which is effectively an implementation of record dynamics in real space. The model and its results are discussed in detail in Sections 2.4 and 6.2.

2.3   Results from experimental data

2.3.1   Statistics of record-sized events

The first key property of the experimental data of Ref. [30] that we check is that irreversible quakes are generated at a decelerating rate $\lambda(t) \propto 1/t$, like records in any *iid* sequence of independent random numbers. Such events were identified as movements of particles involving a replacement of at least three nearest neighbors, shown in Fig. 2a of Ref. [30]. In our Fig. 2.1, we bin the same data logarithmically and see that, over more than three decades, the rate of irreversible events decelerates as $1/t_{\mathrm{w}}$, with time t_{w} elapsed after the quench. Only an initial period of ~ 0.1s, consistent with the time needed for the quench, shows significant deviations from the record-dynamics prediction. To obtain the data, Yunker et al. [30] had to filter out the "in-cage rattle", apparent from the inset of their Fig. 2a. This point is also emphasized by their Fig. 2b, that shows that a slow but steady increase of the domain-size of correlated events can be detected if reversible fluctuations are removed. Unfortunately, the sub-linear but perceptible growth in the relevant regime, i.e., for times > 0.1s, can not conclusively shown to be logarithmic with time, as record dynamics would predict [149, 150]. We test this prediction through a mobility correlation function in Section 2.3.4.

2.3.2   Mean-square displacement

As significant particle motion is activated by these quake events, the distance traveled is proportional to the integral of the rate $\lambda(t) \sim 1/t$. Thus, the mean square
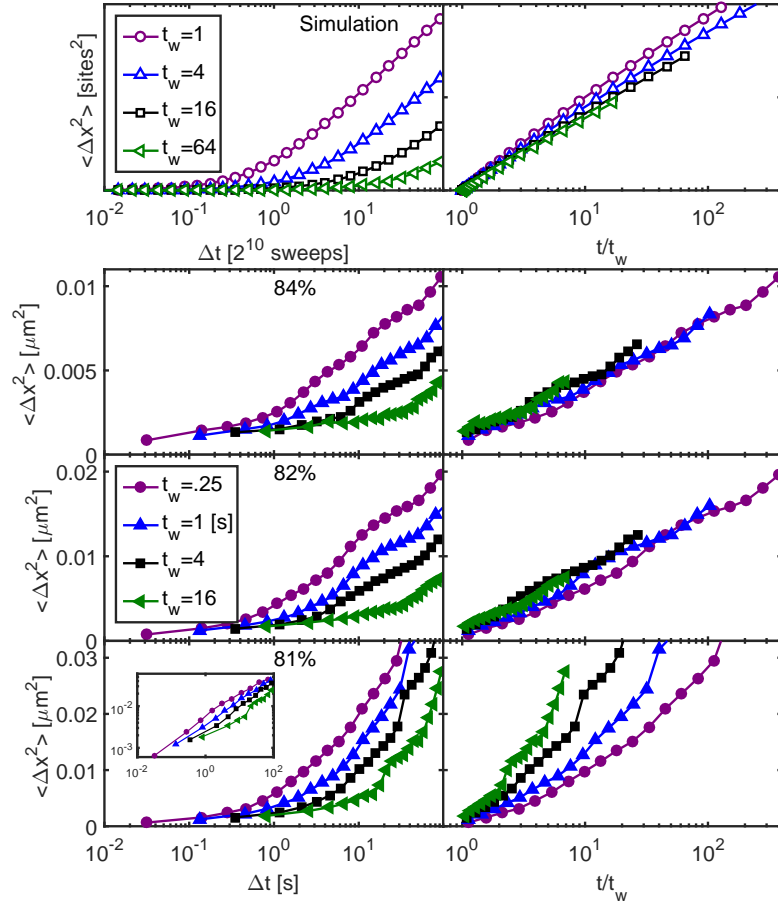
Figure 2.3: Mean square displacement in simulations of the cluster model and in the experiments [30] on aging colloids at several area fractions. Panels of the same row contain the exact same data, however, each panel in the left column is plotted against the conventional lag-time $\Delta t = t - t_{\mathrm{w}}$, and against the logarithmic time-ratio $\ln(t/t_{\mathrm{w}})$ suggested by record dynamics in the right column. The top row shows the simulation data, and the bottom three rows are experimental data arranged by decreasing area fractions, with $\approx 84\%$, $\approx 82\%$, and $\approx 81\%$, from top to bottom. Time units for simulation data are in multiples of 2^{10} Monte Carlo sweeps, to avoid transients after the quench in the early decades. The inset to the bottom left panel contains the same data as that panel, but plotted on a log-log scale.

displacement (MSD) of particles moving between times t_{w} and $t \geq t_{\mathrm{w}}$ in a dense colloid is predicted by record dynamics [149, 152] to grow as $\langle \Delta x^2(t, t_{\mathrm{w}}) \rangle \propto \ln(t/t_{\mathrm{w}})$, where both time-arguments are counted from the initial quench. This 'logarithmic diffusion' was observed in Ref. [149] using particle track data by Courtland and Weeks [148] and is present in the cluster model discussed in Ref. [150]. However, tradition dictates that colloidal data be plotted versus the time-lag $\Delta t = t - t_{\mathrm{w}}$. Using this variable, one easily obtains $\langle \Delta x^2(\Delta t) \rangle \propto \ln(1 + \Delta t/t_{\mathrm{w}})$. Hence, as a function of Δt, the MSD grows linearly as $\sim \Delta t/t_{\mathrm{w}} \ll 1$ and as $\sim -\ln t_{\mathrm{w}} + \ln \Delta t$ for $\Delta t \gg t_{\mathrm{w}}$.

In Fig. 2.3, we observe this behavior in the particle tracking data of Ref. [30] at the highest area fractions, 84% and 82%, deep in the glass phase. The left-hand panel shows that the MSD grows initially weakly as $\sim \Delta t/t_{\mathrm{w}}$, then crosses over for $\Delta t \gg t_{\mathrm{w}}$ to the predicted logarithmic growth. The right-hand panel of Fig. 2.3 shows that the MSD data for different t_{w} and t can, indeed, be collapsed by plotting them as functions of t/t_{w}. As we discuss in Section 2.3.5, the collapse with t/t_{w} remains valid at other jammed packing fractions while the logarithmic slope of the plot increases with decreasing packing fraction. Only at densities too close to unjamming does the collapse begin to fail.

2.3.3 Persistence

Not considered in Ref. [30] is the decay of the persistence, i.e., the probability that a particle does not experience irreversible motion between times t_{w} and t. This quantity gives a clear picture of the spatial heterogeneity of glassy systems: If particle motion follows a regular Poisson process, the persistence decays exponentially in

$\Delta t = t - t_{\mathrm{w}}$. In a log-Poisson process, this becomes an exponential in $\ln(t/t_{\mathrm{w}})$, leading to a power-law decay in t/t_{w}. This prediction was already borne out by simulations of jammed Lennard-Jones systems [166], plotted as a function of lag-time Δt for different waiting times t_{w}. There, after an initial plateau for $\Delta t \ll t_{\mathrm{w}}$, the data decays as a power law for $\Delta t \gg t_{\mathrm{w}}$. Analogous data from cluster-model simulations [150] have reproduced this behavior from the record dynamics and demonstrated a successful collapse of the data as a function t/t_{w}.

In the lower panels of Fig. 2.4, we show the experimental persistence data, plotted as functions of both, the lag time and t/t_{w}, for several system ages t_{w}. Here, a threshold of 0.4μm was used to separate reversible in-cage motion from a significant displacement after t_{w}. As for MSD in Fig. 2.3, at the highest area fractions, 84% and 82%, the data for the jammed system collapses on a t/t_{w}-scale, but here in form of the predicted power-law. Overall, the relaxation dynamics is faster for less-jammed systems, such as that at 81% area fraction shown in the lowest panels of Fig. 2.4. However, the persistence collapse does not break down as much at the packing fraction near unjamming when compared to the MSD. This might reflect the fact that supercooled systems already exhibit considerable heterogeneity [113].

2.3.4 Mobility correlations

In Ref. [30], the size of rearrangement events was characterized by the number of contiguous particles with unusually large displacements. While this approach is reasonable and common for detecting the presence of dynamic heterogeneity in tracking experiments, more precision is required to verify if the growth of event sizes with age

corresponds to record dynamics. Therefore, the mobility-mobility correlation function χ_4, widely used for supercooled liquids [18, 167, 168], has been proposed for this purpose [146, 150, 169]; it is calculated as the ensemble variance of the total mobility at *two* times:

$$M(t, t_{\mathrm{w}}) = \frac{1}{N} \sum_i \exp(-|\vec{\mathbf{r}}_i(t) - \vec{\mathbf{r}}_i(t_{\mathrm{w}})|/d), \tag{2.1}$$

where $d = 0.4\mu$m is a typical length scale to distinguish mobile from immobile particles, here taken to be the same to as the persistence threshold above. The four-point correlation function χ_4 is then defined as

$$\chi_4(t, t_{\mathrm{w}}) = \left\langle M(t, t_{\mathrm{w}})^2 \right\rangle - \left\langle M(t, t_{\mathrm{w}}) \right\rangle^2. \tag{2.2}$$

It is an as-of-yet unconfirmed prediction of record dynamics that the peak of χ_4 grows as $\log t_{\mathrm{w}}$ [150]. Reasoning by analogy with the cluster model, particles that move at time t_{w} belong to collapsing clusters of average size $\sim \log t_{\mathrm{w}}$. The re-activation of those particles requires that a cluster of the same size is reformed and collapses. Such process requires a time-interval Δt_{peak} beyond t_{w} that grows monotonically with t_{w}: For times much shorter than Δt_{peak}, too few particles have a chance of reactivation, while for times much longer than Δt_{peak} most of them already did re-activate and, hence, de-correlate from their mobility at t_{w}. For the experimental data, consisting of single runs, there is no suitable ensemble to average over, so χ_4 is approximated here by dividing a sample into four quadrants and taking the variance across those. This measure is plotted in Fig. 2.5. There are large fluctuations in χ_4 due to the unavoidable interdependence of the regions within a sample and the lack

of statistics. In spite of this, the curves for different waiting times show regularly increasing peak heights for exponentially increasing waiting times, as predicted in simulations of record dynamics [150], also shown in Fig. 2.5.

2.3.5 Data at lower area fraction

The data from Ref. [30] can be used to test the robustness of record dynamics over a range of area fractions. We have stated that specifics of a system do not impact the schematic description of the free energy landscape in Fig. 2.2, as long as the system is jammed. Indeed, the experimental data for the fully jammed systems at the two area fractions $\approx 84\%$ and $\approx 82\%$ in Figs. 2.3-2.4 both show identical behavior for MSD as well as for persistence but for a different unit of time. Thus, only the slopes for the respective collapse of the data is affected (note the scale on each y-axis), indicating less MSD and more persistence within a fixed amount of lag-time for denser systems.

The bottom panels of the same figures refer to a system at an area fraction of $\approx 81\%$, whose behavior is consistent with being unjammed or being too near to the jamming transition. Thus, record dynamics is not expected to apply. In fact, the inset of the bottom left panel of Fig. 2.3 shows that the MSD exhibits nearly linear scaling vs. Δt, which is nearly diffusive behavior. Due to a weak t_w dependence, the MSD data do not collapse when plotted against $\ln(t/t_\mathrm{w})$ in the rightmost panel. However, the data collapse in the bottom panels of Fig. 2.4 suggests that a semblance of dynamic heterogeneity is retained near the jamming transition in the persistence data.

2.4   Comparison with simulations of the cluster model

Becker et al [150] simulated aging over 15 decades using a real-space implementation of record dynamics called the 'cluster model'. The details of the model are discussed in Section 6.2, but in short the model considers clusters of immobile particles which have a small chance to break up and join other clusters. This process yields a breakup event rate proportional to $1/t$ and an average cluster size proportional to $\ln t$. The $1/t$ event rate is observed in the experimental data in Fig. 2.1. The growth of cluster size is a prediction of record dynamics that is consistent with observations of cluster sizes of fast particle in Fig. 2b in Ref. [30].

Here, the mean square displacement and persistence curves obtained from simulations are restricted to 3 decades of scaling to match the range of the experiments. When plotted against lag-time, shown in the upper left panel of Fig. 2.3, the simulation MSD exhibits the commonly expected plateau for $\Delta t \ll t_{\mathrm{w}}$ and rise for $\Delta t \gg t_{\mathrm{w}}$. Averaged over so many runs that error bars become invisible, the simulation curves clearly demonstrate the logarithmic behavior expected from record dynamics. The plateaus in the experimental data at high area fractions in Fig. 2.3 have a slight slope $\sim \Delta t/t_{\mathrm{w}} \ll 1$ due to the in-cage motion. Both the simulation and experimental data collapse to a uniform logarithmic growth at all t_{w} when plotted against t/t_{w}.

Persistence in the simulation is calculated as the fraction of particles that have not moved to a different lattice site. As with the MSD, due to the lack of in-cage rattle, the systems appear frozen for lag-times shorter than the waiting time. The persistence data from simulations shown in the top row of Fig. 2.4 demonstrate the power-law decay predicted by record dynamics. For the experimental data, a suitable

metric had to be determined to classify particles as persistent. It was found that setting a distance threshold and taking the fraction of particles that move beyond that distance from their position at t_{w}, robustly yields results qualitatively similar to the simulation curves. The experimental persistence curves shown here are all produced using a threshold of $0.4\mu\mathrm{m}$.

2.5   Conclusions

Our detailed analysis of the experimental particle tracking data of Yunker et al. [30] *i)* satisfies that the rate of irreversible particle rearrangements falls off as the inverse of the system age; *ii)* Confirms [149] that the positional variance due to particle motion between t_{w} and t grows as $\ln t/t_{\mathrm{w}}$, a diffusive behavior in the logarithm of time; *iii)* Shows that persistence data can be scaled in the same way, as function of t/t_{w}; *iv)* Shows that the peak of the four-point susceptibility $\chi_4\left(t, t_{\mathrm{w}}\right)$ grows in a way consistent with $\ln t_{\mathrm{w}}$; *v)* Confirms that the range of applicability of record dynamics is, as predicted, limited to sufficiently dense colloidal systems. Finally, the analysis of the experimental data concurs simulational data from our 'cluster model' [149, 150].

The agreement between experimental data and record dynamics predictions for all packing fractions in the jammed regime (and only there) confirms that aging dynamics is controlled in each instance by a small set of active variables, which move intermittently in time. That such variables cluster in space is well known as spatial heterogeneity and can be seen in the data of Ref. [30]. Even though more accurate experimental measurement of χ_4 are required to ascertain whether the clusters grow logarithmically in time, there is clear experimental evidence that they do grow.

Continuous Time Random Walks (CTRW) are most widely used to coarse-grain the dynamics of systems jumping from trap to trap via rare intermittent events, see e.g. [162]. Confusingly, CTRW and RD predictions are partly overlapping, while their physical mechanisms are very different. Importantly, as will be argued in Chapter 4, CTRW are for a number of reasons inadequate descriptions of aging [152]. Here we can only add that the emergence of a growing physical length scale suffices to rule out a renewal process as the underlying mechanism for aging in dense colloids. Real-space mesoscopic objects whose lifetime grows exponentially with their size or, equivalently, whose characteristic length grows logarithmically in time, are arguably a key feature of off-equilibrium glassy dynamics and deserve further experimental investigation.

We will further discriminate between the CTRW picture and record dynamics in Chapter 4 by considering the statistics of irreversible event times. However, this discrimination requires more statistics than are available in these 3000-particle windows, and will require a robust definition of such an event. To those ends, in Chapter 3 we develop molecular dynamics simulations of aging colloids to study large aging colloidal systems.
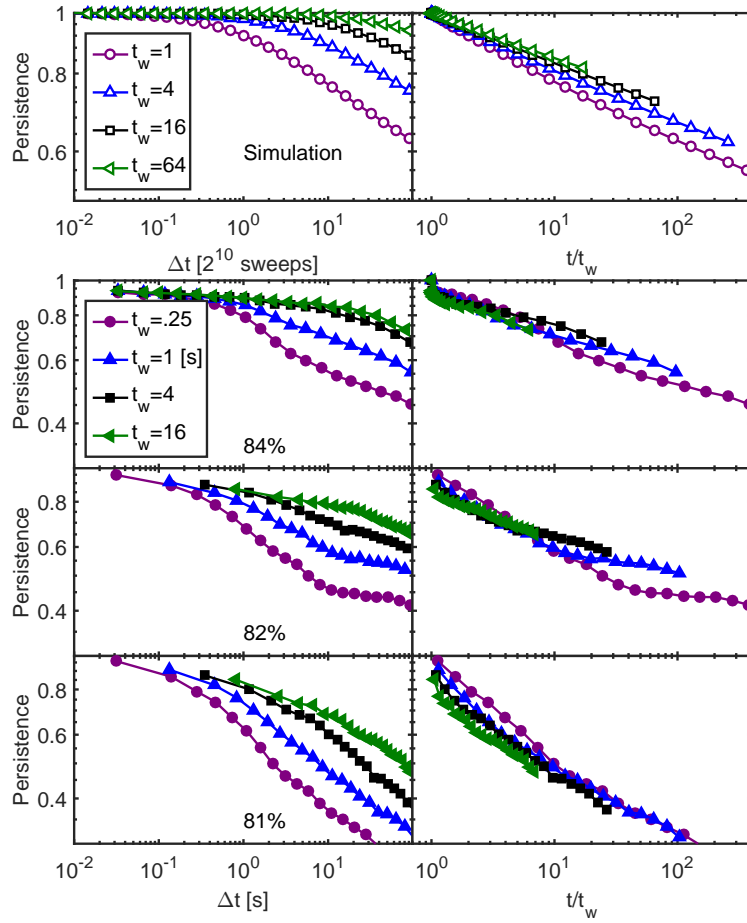
Figure 2.4: Persistence in cluster model simulations and in the experiments [30] on aging colloids at several area fractions. Persistence is measured as the fraction of particles with displacements less than $0.4\mu m$. The arrangement of panels is identical to that of Fig. 2.3.
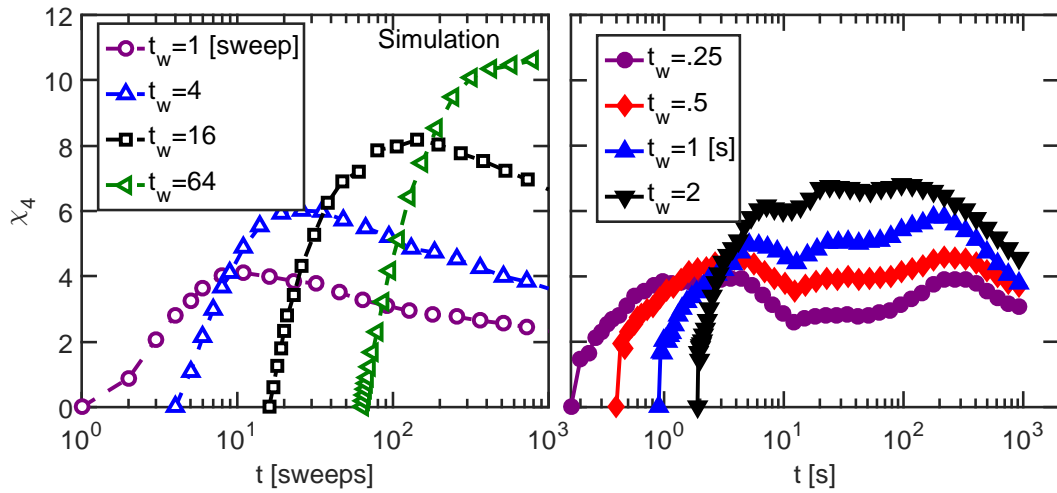
Figure 2.5: Growth of length scale of dynamic heterogeneity as measured by the four-point susceptibility $\chi_4\left(t, t_{\mathrm{w}}\right)$, which is a measure of the mobile particles at time t that had been mobile also at time t_{w}. The height of each peak is proportional to the number of particles involved in a significant rearrangement event at time t_{w}. Simulations of the cluster model [150] (left) have shown that the size of those events grows $\sim \ln t_{\mathrm{w}}$, reflected in the peak-height of χ_4. The experimental data (right) shows a discernible peak growing monotonically with t_{w} in an approximately logarithmic manner consistent with the record dynamics prediction.

Chapter 3

Two-time dynamics in a simulated colloidal glass

3.1 Introduction

During aging, observables retain a memory of the waiting time t_w since the quench, signifying the breaking of time-translational invariance and the non-equilibrium nature of the state. For example, measures of the activity within the system taken over some time-window $\Delta t = t - t_w$, such as the van-Hove distribution of particle displacements, are now a function of two time-scales, Δt and t_w, instead of just the lag-time Δt, as would be the case in a steady state. As has been observed previously [113, 116, 137, 166], those distributions are characterized by broadened, non-Fickian tails that get broader with time Δt, but each in a manner that is characteristic of its age. Those tails clearly emphasize the fact that anomalously large fluctuations in the displacement of particles drive the structural relaxation, which proves intimately

related [149, 150] to the spatial dynamic heterogeneity as well as the temporal intermittency that have been observed in many experiments [30, 31, 113, 134–137, 141–143, 170]. The dynamic events of interest are therefore rare and non-self-averaging, requiring many independent simulations of large systems to yield clear results. Further, examination of both short and long time scales requires both a high temporal resolution and long simulation runs. For these reasons, an experimental study of an aging colloidal system on *two* timescales with sufficient accuracy is a daunting task and has not been attempted yet.

In this chapter, we measure the two-time behavior of the fundamental van-Hove distribution of particle displacements during aging, provide a scaling collapse of the data, and comprehensively explain our observations in terms of the preeminence of intermittent, record-sized events. To this end, we reconstruct the setting of the simplest of such an experiment [30], a planar bi-disperse colloid quenched rapidly into a jammed state, as a molecular dynamics simulation. In our simulations we first reproduce previously published results of the experiment for mean-square displacements of particles in great detail. Using an equivalent criterion to identify irreversible relaxation events as in Ref. [30], we find in particular that the rate of such events declines with age as $\sim 1/t$, shown also for the experimental data from Chapter 2. Those results demonstrate that the simulation significantly extends the accuracy of the measurements by using a large number of instances. Then, we present results for the particle displacement distribution, i.e., the van-Hove function, that indeed reveal a dependence on both Δt and t_w, indicative of aging. The distribution of displacements spreads out with increasing Δt, as one would expect in any relaxing system.

However, if Δt is fixed but t_w is increased, the distribution narrows, demonstrating the decreasing activity due to structural changes during aging. The data readily collapses as a function of $\Delta t/t_w$ over a wide range of times. By the fundamental nature of the van-Hove function [171], this implies similar scaling in many other observables. We finally show that all of these results can be reproduced with a recently proposed lattice model [150] based on the simple fact that the relaxation dynamics requires ever larger (record-sized) fluctuations in the cluster of activated particles [149, 156, 165].

3.2 Simulation details

The simulations of the colloidal system are performed using the Python molecular dynamics package HOOMD-Blue [172, 173]. Each simulation contains 100,000 particles with periodic boundary conditions. The particles form a 50/50 bidisperse mixture with diameter ratio 1.4. Trajectories are computed using Newtonian integration with a harmonic repulsive interaction potential given by $E(r_1, r_2) = \epsilon \left(|\mathbf{r_1} - \mathbf{r_2}| - r_1 - r_2 \right)^2$, where $\mathbf{r_1}$ and $\mathbf{r_2}$ are the positions of particles 1 and 2, and r_1 and r_2 are their radii. The simulation temperature and particle interaction strength ϵ are chosen to make dynamic time and length scales comparable to previous work. Specifically, we matched the particle size ratio and packing fraction of Ref. [30]. The simulations are run at 74% packing fraction for 5 seconds, which is empirically found to equilibrate the system. The simulation temperature determines the distribution of particle velocities. This distribution determines the diffusion constant in this equilibrated fluid regime. We tuned the temperature to make particles diffuse by one diameter in one simulation time unit, to match the 1 second diffusion of the experimental colloid in Ref. [30], so

we refer to the simulation time unit as a second. Then the simulation box is rapidly compressed in .1s to a packing fraction of 84%. We then record particle positions every .01s for 20s. This protocol is repeated for 10 independent realizations.

All particles in our simulations obviously experience many collisions during a simulation, most of which restrain a particle to a local "cage" formed by the tight constraints its neighbors impose on its mobility [113]. After some time particles might spontaneously undergo a cooperative rearrangement. Such a rearrangement is noticeable in a single particle's trajectory as a shift to a new position. It is noteworthy that the distance traveled to a new cage is usually within the normal range of in-cage rattling displacements, making the distinction between the two types of motion a subtle one. In fact, the difference in a particle's position before and after a rearrangement can be less than 10% of its diameter and only changes in the neighborhood topology (as detectable by a Voronoi tessellation, discussed in Section 3.4) may suffice to qualify such a displacement as irreversible (see below). Nevertheless, we argue that these spontaneous rearrangements are the mechanism responsible for aging in glassy systems.

3.3   Mean squared displacement

Simulation results for the system-averaged mean squared displacement (MSD) starting from different waiting times are shown in Fig. 3.1(a). MSD is usually considered as a function of waiting time t_w and lag-time $\Delta t = t - t_w$, as shown. The system demonstrates the typical plateau associated with caging, followed by diffusion on longer time scales as cages are escaped. The height of the plateau suggests a caging
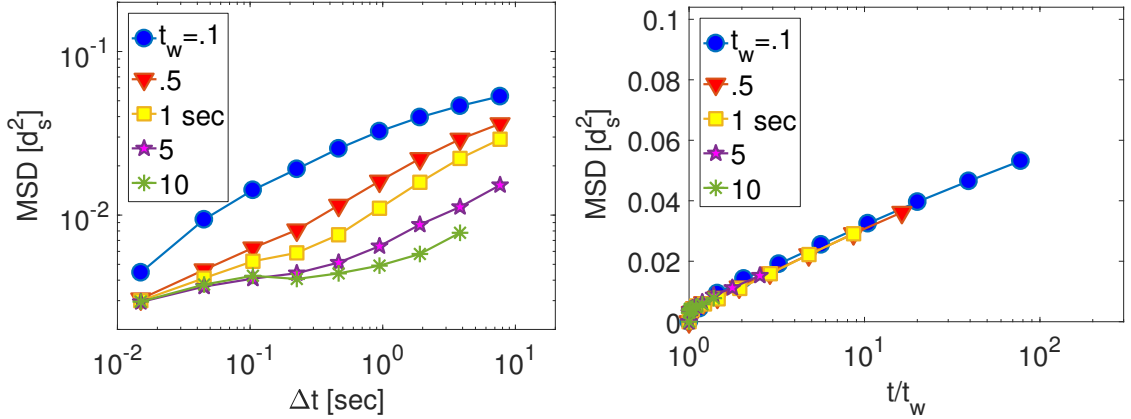
Figure 3.1: (a) Mean Squared Displacement (MSD) in units of d_s^2, where d_s is the diameter of the small particles. plotted as a function of lag-time $\Delta t = t - t_w$ when the MSD is measured starting at age t_w. It shows how a glass stagnates with age. (b) A collapse of the data from (a) shows that the MSD is invariant with respect to t/t_w. These simulation results closely resembles the behavior of the experimental data from Yunker et al [30] as shown in Figure 2.1.

length scale between about 1% and 10% of a particle diameter. Beyond that, the dynamics is driven by activated events and the particles intermittently move $> 10\%$ of a diameter. These ranges are consistent with the trajectories seen in Ref. [30]. We also see the plateaus getting longer with increased t_w. For very early waiting times, the cages are so short-lived that there is no apparent plateau, but the growing caging time scale is still apparent as a shift in the diffusive part of the curve. It should be noted that the word "diffusive" is used loosely here. If the MSD curves were truncated earlier, then one could mistake the upturn in them for straight lines on a log-log scale, see Fig. 3.1(a). However, on longer time scales, the curves for the earlier waiting times begin to level off. We do not consider this as the approach to another plateau, but rather indicative of the nature of physical aging. If cooperative rearrangements are due to record-breaking fluctuations, and each rearrangement between t_w and t
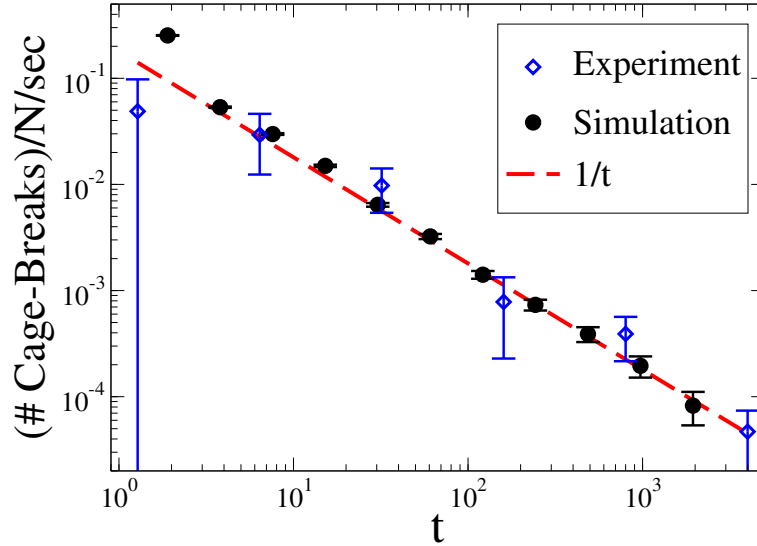
Figure 3.2: Decay in the rate of irreversible neighborhood swaps in a jammed colloid in the simulations. Overlaid is the corresponding experimental data for intermittent cage-breaks ("quakes") from Fig. 2a of Yunker et al [30], as previously discussed in Ref. [174]. The data is consistent with the hyperbolic decay, $\sim 1/t$ (dashed line), predicted by record dynamics [150].

ratchets up the MSD, then the MSD increases roughly logarithmically with Δt as in Chapter 2 and Ref. [150], as explained via Eq. (3.2) below. This expectation is verified by Fig. 3.1(b), which shows the exact same MSD data collapsed when plotted as function of $\log(t/t_w)$.

3.4 Distinguishing rearrangement events

Measurement of the rate at which cooperative rearrangements occur requires some sort of discretization of the system dynamics. The distribution of particle displacements itself does not easily allow for discrimination between caged and rearranging particles. As we will discuss below that distribution is characterized by a Gaussian

core at shorter distances and an exponential tail further out, with merely a gradual transition between them, see Fig. 3.3. The exponential tail has been attributed to rearranging particles, but may also be due to heterogeneity in cage sizes [175]. These facts make rearrangement detection based on particle displacements dubious. However, subtle changes in the configuration can be detected by considering changes among neighboring particles. To that end, the radical Voronoi tessellation is computed for each frame of six simulations using the C++ library Voro++ [176].

The Voronoi tesselation of a space defines regions of that space based on their proximity to a particle. A region of space which is closer to a particle's center than it is to any other particle is called that particle's Voronoi cell. Cells which share an edge are called neighbors. Since our particles are different sizes, we use the radical Voronoi tessalation, which considers distance from the surface of a particle instead of the center.

A history is constructed of every pair of particles which are neighbors at any point in the simulation. For each neighbor pair, the first frame of the simulation in which that pair are neighbors is also recorded. In this manner, a particle which never rearranges in the entire simulation would have roughly six *new* neighbors in the first frame, then none for the rest of the simulation. When a rearrangement occurs, the Voronoi tessellation changes, and a few particles encounter new neighbors. Reversible in-cage fluctuations might create flickering Voronoi networks, but these changes can be shaken out in a few frames by only counting the *first* contact with a neighbor. Not all particles in a rearranging region will make new contacts, and some rearrangements send particles back to old neighbors, but as long as a consistent fraction of rearranging

particles encounter new neighbors, a count of the new neighbors in a given frame is a reasonable measure of the rearrangement event rate.

For their particle tracking experiments, Yunker et al [30] also defined irreversible neighborhood swaps that were shown to decay with time after the quench. Simply binning their data logarithmically, it was shown in Chapter 2 that the experimental rate of those events decays with age in a manner that is consistent with $\sim 1/t$. Using the Voronoi method described above, we determine the corresponding event rate in the simulations to find a perfect match with that experimental data, see Fig. 3.2. Moreover, due to the ability to rerun the simulation many times, the decay in the rate appears to be hyperbolic to a high degree of statistical significance.

3.5 Displacement distribution

Going beyond mere comparisons with existing experimental results, we can now use our simulation to study two-time correlations that are difficult to access with sufficient accuracy in experiments. For example, in Fig. 3.3 we show results for the single-axis particle displacement distribution over a time-window Δt starting at t_w,

$$G_s\left(\Delta x, t_w, \Delta t\right) = \sum_i \delta\left(\left|x_i\left(t_w + \Delta t\right) - x_i\left(t_w\right)\right| - \Delta x\right), \qquad (3.1)$$

also known as the self-part of the van Hove function [171]. Here $\delta(x)$ is the Dirac delta function. In our simulations, for $\Delta t < .001$s (not shown), few collisions have occurred, so the distribution of displacements would be largely due to the distribution of particle velocities. On intermediate time scales, $\Delta t \approx .01$s, the distribution is determined by the cage size distribution. On longer time scales, the distribution begins to spread
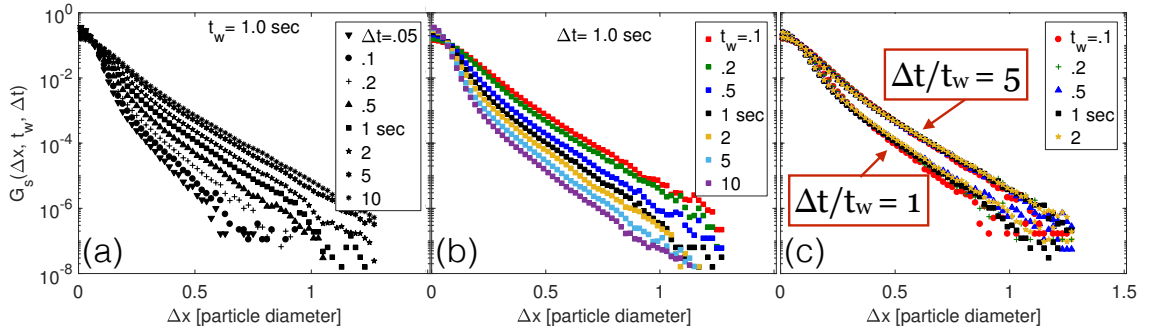
Figure 3.3: Distribution of single particle displacements $G_s(\Delta x, t_w, \Delta t)$ in the simulations (self-part of van-Hove function), as defined in Eq. (3.1). (a) The distribution spreads out *more* with increasing Δt (different symbols) at some fixed waiting time $t_w = 1s$. (b) The distribution spreads out *less* over a fixed time window Δt with increasing t_w (different colors). (c) These distributions collapse for fixed ratios of $\Delta t/t_w$, as predicted by record dynamics, see Fig. 3.4.

out, as previously observed in similar simulations in Ref. [166, 177], for example. In Fig. 3.3(a) for $t_w \approx 1$s, this spreading begins at around .1s, but the spreading begins later with increasing t_w.

Note that G_s in Fig. 3.3 exhibits exponential "non-Fickian" tails, beyond the dominant Gaussian fluctuations at short distances, that signify rare intermittent behavior, similar to observations in spin-glass simulations [87, 139, 140]. It has been measured previously in various colloidal experiments and simulations [64, 113, 116, 137, 166, 175, 178], but averaged over long time intervals that blend together various waiting times t_w, and never considered as a function of both t and t_w. While the shape of G_s is generally invariant, the weight of this tail increases with Δt, but it decreases with age t_w, since activated cage rearrangements become increasingly harder. Amazingly, all data collapses when the time-window Δt is rescaled by the age t_w. Similar to the analysis of the MSD in Fig. 3.1(b), by scaling the lag time with the waiting
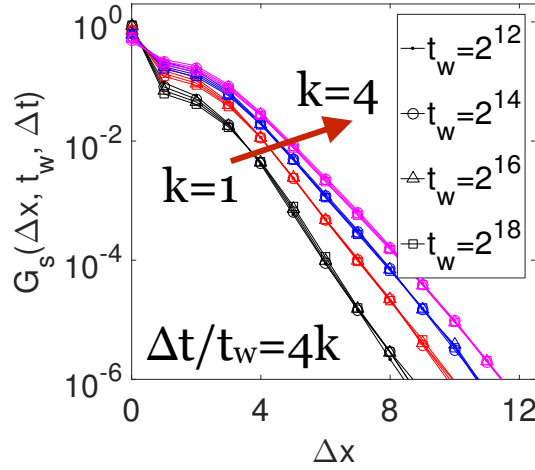
Figure 3.4: Plot of the van-Hove particle displacement distribution G_s in Eq. (3.1) in the cluster model. Note the similarity in the exponentially broadened (non-Fickian) tails compared with the simulation data in Fig. 3.3. Here, G_s is measured at four different waiting times t_w (different symbols), each over four different time-windows $\Delta t = t - t_w$ (different colors) such that $\Delta t/t_w = 4k$ with $k = 1, \ldots, 4$. For each k, the respective data collapse.

time, we should observe the same number of rearrangements for any given $\Delta t/t_w$, if the rearrangements correspond to record breaking fluctuations. In Fig. 3.3, two collections of curves are plotted accordingly, one set with $\Delta t/t_w = 1$, and another with $\Delta t/t_w = 5$. Note that many common dynamical observables, such as MSD or the self-intermediate scattering function (and, thus, the persistence [166][150, 174]) can be calculated from the van Hove function [171]. In demonstrating the collapse of G_s, we have shown that all measures involving averages over single-particle displacements would collapse similarly. The collapse of these curves suggests that the dynamics of this aging system is driven by record-sized fluctuations: if $\Delta t \ll t_w$, quasi-equilibrium in-cage rattle dominates while rare, intermittent and irreversible cage-breaks encountered for $\Delta t \gtrsim t_w$ drive the actual non-equilibrium relaxation pro-

cess. As these break-ups require record-sized fluctuations that decelerate with $\sim 1/t$, the statistics is invariant for $\Delta t/t_w$, as the following considerations explain.

3.6   Discussion

In the experiment and simulations, anomalously large cage break events are found to substantially relax the system and must be viewed as distinct from the Gaussian fluctuations of in-cage rattle. Yet, such a relaxation must entail a structural change, which makes subsequent relaxations even harder. For example, to facilitate a cage-break, Yunker et al [30] observed that a certain number of surrounding particles have to conspire via some rare, random fluctuation. For that event to qualify as irreversible, the resulting structure must have increased stability, however marginal. A following cage-break thus requires even more particles to conspire. With each of those fluctuations exponentially unlikely in the number of participating particles [64], cage-breaks represent *records* in an independent sequence of random events that "set the clock" for the activated dynamics. In such a statistic, record events are produced at a *decelerating* rate of $\lambda(t) \propto 1/t$, consistent with the results in Fig. 3.2. As those records do not cause each other, we obtain a log-Poisson statistics, for which the average number of intermittent events in an interval $t_w < t < t_w + \Delta t$ is

$$\langle n_I\left(\Delta t, t_w\right)\rangle \propto \int_{t_w}^{t_w+\Delta t} \lambda(\tau)\, d\tau \propto \ln\left(1 + \Delta t/t_w\right), \tag{3.2}$$

which explicitly depends on the age t_w. Then, any two-time observable, like the van-Hove distribution in Eq. (3.1), becomes *subordinate [141]* to this clock: $G_s\left(\Delta t, t_w\right) = G_s\left[n_I\right] = G_s\left(\Delta t/t_w\right)$. In reference to a Poisson statistic, where a constant rate λ

provides time-translational invariance (stationarity) with $\langle n_I \rangle \propto t - t_w$, this record dynamics is a log-Poisson process [152]. We have indeed verified the log-Poisson property for our simulations [179]. The generality of this argument may address the astounding commonality in slow relaxation that holds across many glassy systems, quenched and structural, irrespective of microscopic details [174].

To illustrate that record-breaking fluctuations are sufficient to produce the observed dynamics, we also apply our analysis of the van Hove function to the cluster model [150] described in Section 6.2. Following the definition in Eq. (3.1), we have measured G_s also for displacements of particles in this model. Fig. 3.4 shows that this data reproduces the $\Delta t/t_w$-collapse for the van Hove distribution of particle displacements found in the molecular dynamics simulations. Note that even though the Gaussian fluctuations due to in-cage rattle are coarse-grained out in the cluster model, the Gaussian core of G_s is retained. Since each breakup of a large cluster results in a series of smaller breakup events, particles have opportunity to diffuse briefly before locking into a new cluster. Note also the sharp peak at $\Delta x = 0$ due to particles which have not rearranged at all.

3.7 Outlook

In future simulations, we intend to analyze the effect on aging of varying the density attained after a quench. As in the experiments, we expect that those variations (above a certain threshold of about 81%) will merely affect some pre-factors numerically without changing the log-Poisson characteristic of the aging discussed in Chapters 2 and 4. The corresponding variation in the cluster model is achieved

by varying the exponential in $P(h)$, which affects each observable there. Finding a response to such variation that is equivalent for *all* observables between cluster model and molecular dynamics simulation provides a substantial test for the record dynamics interpretation.

Chapter 4

Log-Poisson nature of physical aging

4.1 Introduction

The phenomena observed in Chapters 2 and 3 were described in term of the 'record dynamics' framework. Another popular approach is to treat aging as a renewal process [180–184]. In the trap model [180], for instance, the entire system performs a random walk through a configuration space filled with traps possessing a broad (power-law) distribution of escape times. Thus, the older the system, encountering ever "deeper" traps will become more likely, and the deepest trap encountered dominates all previous timescales. However, once escaped, no memory of previous events informs future events. As noted in Ref. [152], applying this type of description to aging systems violates the system size scaling and self-averaging properties of macroscopic variables, which are universally observed in nature. The problem is avoided
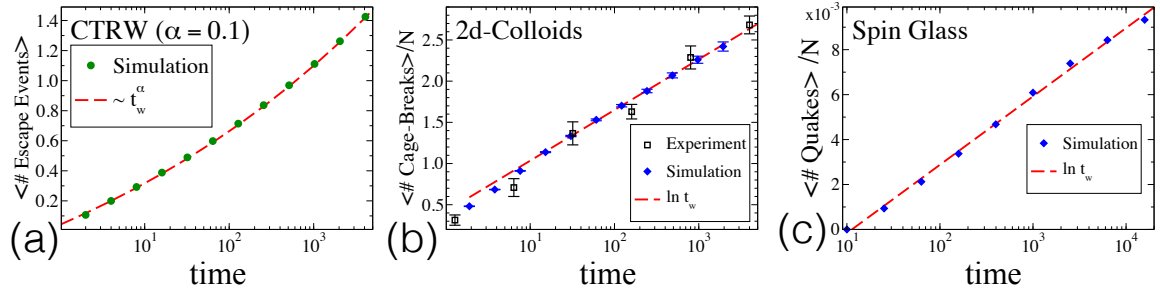
Figure 4.1: Accumulated number of relaxation events ("quakes") with time t after a quench during simulations of (a) a continuous-time random walk (CTRW), (b) a jammed *2d* colloids, and (c) a *3d* Edwards-Anderson spin glass. In (a), we sampled the number of escapes by evolving Eq. (4.2) for a rather small value of $\alpha = 0.1$, to more closely resemble the physical aging data in (b-c). In (b) molecular-dynamics simulation data from Chapter 3 and colloidal experiment by Yunker et al [30] from Chapter 2. In (c), we obtained the irreversible barrier crossings in a *3d* Edwards-Anderson spin glass. Note that the physical data is growing logarithmically with time, while such a behavior is obtained in the CTRW only for $\alpha \to 0$.

in continuous-time random walks models (CTRW), where each particle in a colloid, say, is now endowed with a power-law distribution of times between displacements. Over time, particles perform intermittent jumps, interpreted as them breaking out of their cages formed by surrounding particles, as particle-tracking observations tend to justify [113, 116].

In this chapter we show, however, that any such renewal process is ruled out as an underlying physical mechanism by demonstrating that the transitions from one metastable state to the next follow a log-Poisson process which originates from the record-sized fluctuations needed to relax the aging system.
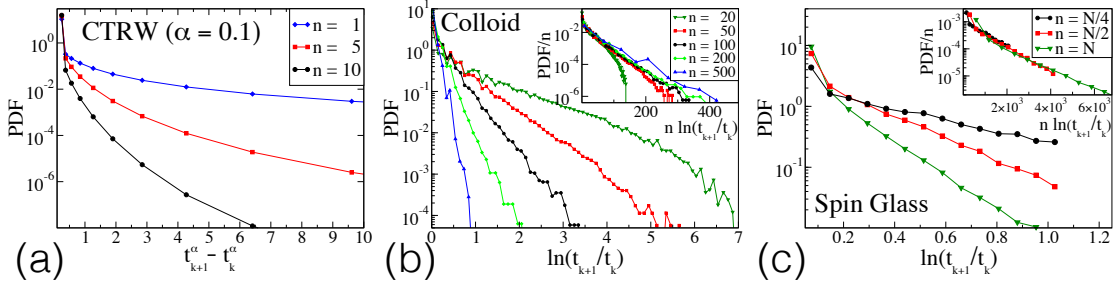
Figure 4.2: Poisson statistics of (a) the CTRW in Eqs. (4.1-4.2) for $\alpha = 0.1$, and for the aging dynamics in simulations of (b) a colloid and (c) a spin glass. Times t_k mark the kth event, i.e., escaping a trap in the CTRW, an irreversible cage-break in a colloid, or quakes in a spin glass. The CTRW does not have the exponential form expected for a Poisson process, while both physical aging processes do. Generally, when too many events (i.e., too many degrees of freedom) are blurred together, it hides the local impact of the decelerating activated events and tails weaken. Record dynamics predicts that the rate of events is proportional to the number n of degrees of freedom observed. As the inset for both, (b) and (c), shows, the data in the aging simulations indeed collapse when rescaled by n.

4.2 Deceleration in a renewal process

By their very nature, renewal processes seem antithetical to aging because each renewal resets the history. However, it is the broad distribution of escape times that ensnares an increasing number of particles for indefinitely long times after the quench and overall activity decelerates. To be specific, the probability for observing m such cage-breaking events after the waiting-time t_w since the quench in a single CTRW is given by

$$p_m \left(t_w \right) = \int_0^{t_w} d\tau \, p_{m-1} \left(t_w - \tau \right) \psi \left(\tau \right), \tag{4.1}$$

initiated with $p_m(0) = \delta_{m,0}$, and an inter-event-time distribution

$$\psi(\tau) \sim \tau^{-1-\alpha}, \qquad (0 < \alpha \le 1). \tag{4.2}$$

For such α, inter-event times, i.e., escape times, have a diverging mean and the rate at which events are observed, $\partial_t \langle m \rangle \sim t_w^{-1+\alpha}$, indeed decelerates, so that the accumulated number of events rises sub-linearly, see Fig. 4.1a. Moreover, when such a process has evolved up to time t_w after the quench, the probability to observe the next (escape) event within a time-interval $\Delta t = t - t_w$ exhibits the t/t_w-dependence [1] characteristic of most aging phenomena [182]: As the time needed to escape the typical trap entered at t_w is itself $\propto t_w$, then so is $\Delta t \propto t_w$, which constitutes some fraction of the total escape time. These are powerful features of renewal models that have contributed greatly to justify their widespread application to fit data produced in a wide variety of aging experiments [26, 116, 180, 183, 187–189]. The exponent α provides a readily available parameter to fit data. However, the *physical* origin of α or $\psi(\tau)$ is unclear.

4.3   Irreversible event rates

In light of its potential benefits, it is most instructive to compare CTRW with a direct measure of the sequence of quake events in realistic aging processes, to assess their statistical properties more fully. This we have undertaken in molecular-dynamics

---

[1]At the level of macroscopic observables, this t/t_w-dependence is however only approximate. Macroscopic data are often empirically scaled using 'sub-aging', which is a cross-over phenomenon [185] on top of the Record Dynamics mechanism, as discussed in "Origin of 'end of aging' and sub-aging scaling behavior in glassy dynamics" [186].

simulations of a *2d* system of bi-disperse colloidal particles and a Monte Carlo simulation of $3d$ Edwards-Anderson spin glasses. (Details of these simulations are described in Ref. [190]), and Chapter 3. Each provides a canonical model of aging (and glassy behavior generally) for quite distinct disordered materials [81, 155].

In a colloid, disorder is merely structural, arising from the irregular random packing of the particles [155]. In contrast, in a spin glass, dipolar magnets are localized in a lattice of a-priori fixed but randomly chosen couplings with their neighbors that would frustrate their optimal alignment even in any conceivable – yet dynamically inaccessible – equilibrium arrangement [81]. In both systems we follow the sequence of events after a quench, achieved by either rapidly expanding the colloidal particles to transition from a low-density liquid into a high-density jammed state, or by lowering temperature of the spin glass well below its glass-transition temperature. Sampling over repeated simulations, we have recorded either the cage-breakings or the energy barrier-crossings (see Fig. 4.3), which constitute the irreversible events (or jumps) signifying activated relaxation in the respective systems.

In all three cases the rate of events does decelerate as a power-law with time. However, in both simulations the rate is essentially hyperbolic, $\partial_t \langle m \rangle \sim t_w^{-1}$, such that the accumulated number of events increases logarithmically with time, as plotted in Fig. 4.1. This feature of the physical data a renewal process only achieves in the limit of $\alpha \to 0$. That limit is somewhat singular because the distribution in Eq. (4.2) would become un-normalizable. Arguably, this could be accounted for within numerical accuracy of the data by stipulating logarithmic factors or by simply assuming some small value of α (like $\alpha = 0.1$, as used in Fig. 4.1a). Yet, the following

will demonstrate that the key discrepancy between a renewal model and the data arises from the actual *sequence* of quake events.

Focusing first on the numerical data, we let t_k denote the kth quake in the time series of measured irreversible events extracted from a trajectory. Figs. 4.2b-c show the statistics of the logarithmic time differences $\Delta \ln = \ln t_{k+1} - \ln t_k = \ln (t_{k+1}/t_k)$, which we treat as identically distributed stochastic variables. To wit, to a good approximation, the statistics is described by an exponential probability density function (PDF) $P_{\Delta \ln}(x) = \exp\{-x/\mu_q\}/\mu_q$, which is shown for a number of different system sizes. The rate of events, $1/\mu_q$, increases with system size or simply the number of tracked particles n. That the scaling is indeed linear is shown in the insets, where all data are collapsed by the scaling transformation $\Delta \ln \to \Delta \ln /n$. Thus, the form of the data supports the hypothesis that quake events have a log-Poisson statistic, i.e., the data follow a Poisson distribution whose only parameter – the average – grows *logarithmically* with time, i.e., $\mu_q \propto \ln t$.

The additivity of Poissonian variables now ensures that the number of events is an extensive variable. In CTRW, the number of on-going independent random walks is a fitting parameter rather than a dynamical consequence of the size of the system at hand. One can nevertheless look at the sequence t_k of renewal events generated by n different random walks. For $n = 1$, the PDF of the time intervals $\tau = t_{k+1} - t_k$ between consecutive events at times t_k and t_{k+1} by definition reproduces the power-law distribution $\psi(\tau)$ in Eq. (4.2). For $n > 1$, the data from the renewal process retain a power-law distribution, inconsistent with a Poisson process on any timescale.

Even if we define a generalized α-Poisson process, based on the observation that

the rate of events observed in a renewal process is $\partial_t \langle m \rangle \sim t^{-1+\alpha}$, i.e., $\langle m \rangle (t, t_w) \sim t^\alpha - t_w^\alpha$, the α-intervals between events, $t_{k+1}^\alpha - t_k^\alpha$, remain power-law distributed and distinctly non-Poissonian, as demonstrated in Fig. 4.2a. Thus, a renewal process must be rejected as a model for aging! With further extensions [191], a non-renewal CTRW can be designed that evolves many walkers in parallel, one for each future event. Here the system, after leaving the trap of one walk, immediately enters the already extant trap of another walk, instead of undergoing renewal. While this model provides a log-Poisson statistic for all $0 < \alpha < 1$, any connection to the physical processes we discuss here is tenuous, at best.

4.4   Record dynamics

In contrast, it is quite fruitful to view aging as a record dynamics (RD) [152, 156, 165] as described in Section 3.6. In a statistic of records, a sequence of t independent random numbers drawn from *any* smooth probability density function produces a record-sized number at a rate $\partial_t \langle m \rangle \sim 1/t$. Hence, the number of random events tallied between a time t_w and $t = t_w + \Delta t$ is $\langle m \rangle (t, t_w) \sim \ln(t) - \ln(t_w) \sim f(t/t_w)$. Thus, RD leads to a log-Poisson statistic [152], as found for the physical data above. RD also considers anomalously large events, like cage breaks in colloids, as being essential to substantially relax the system and having to be viewed as distinct from the Gaussian fluctuations of in-cage rattle. (This distinction is also essential to CTRW, as the discussion before Eq. 2 in Ref. [116] shows.) Yet, such a relaxation must entail a structural change – the physical essence of aging – that makes subsequent relaxation even harder, a fact which renewal models ignore, see Fig. 4.3. This figure makes

explicit in a spin glass simulation the diagram of an energy landscape in Figure 2.2.

Yet again we examine the cluster model described in Section 6.2 to demonstrate the behavior of an ideal implementation of record dynamics. While Ref. [150] already obtained a hyperbolic event rate for the cluster model, consistent with Fig. 4.1b-c, in Fig. 4.4 we demonstrate its log-Poisson behavior.

4.5   Conclusions

In conclusion, our study shows that existing models of aging based on renewal processes are inconsistent with the physical evidence of aging exhibiting 'jumps' or 'quakes' describable as a log-Poisson process.

The implications of this finding for other models of aging remain less obvious. Amir et al [88, 192] stipulate a convolution of relaxation rates λ with distribution $P(\lambda) \sim \lambda^{-1}$ that implies aging of observables $\sim \log(t/t_w)$, consistent with our description. Earlier theories [78, 193], derived from mean-field spin glasses before experiments implicated the importance of intermittency [30, 136, 137, 141, 170], describe aging merely as a gradual process. Future analysis will reveal its consistency with the evidence in its system-wide averages, but it lacks any notion of *localized* spatiotemporal heterogeneity now considered essential in the understanding of slow relaxation.

In contrast, a description of jamming in terms of a random first-order transition (RFOT) [194, 195] explains the mechanics of *individual* cage-breaking events in structural glasses in great detail, putting some emphasis on the irreversibility of the event and the structural relaxation it implies. There, the increasing free-energy barriers we stipulated for reaching lower metastable basins in the landscape are explained in

terms of an impending entropy crisis: lower-energy basins are ever harder to find. Yet, we are not aware of any prediction within RFOT about the observed $1/t$-deceleration in the rate of quake events, or any other hallmark of a log-Poisson process. In fact, the need for such a microscopic justification for aging is somewhat antithetical to the rather broad universality found here for both structural as well as quenched glasses, at least for an elementary protocol.
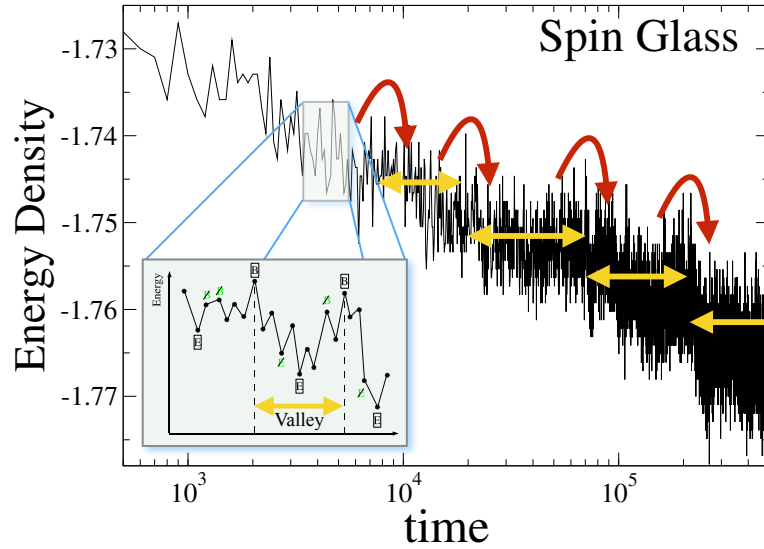
Figure 4.3: Energy trace during a single aging process in a *3d* EA spin glass system with time *t* after a quench. The energy decreases logarithmically with time in a widely fluctuating manner. Unlike in a renewal process, a glass never returns to energy levels visited decades earlier, signifying the gradual but significant structural evolution in the configuration of spins. Energy leaves the systems in intermittent and *irreversible* escape events ("quakes") out of "valleys" (yellow arrows) triggered by a record fluctuation (red arrows). Inset: Tumbling through a complex energy landscape, a time sequence of lowest energy (E) and highest barrier (B) records (relative to the most recent "E") is produced [99, 164]. Only highest and lowest records of the "E and "B" are kept to give a strictly alternating sequence "EBEBE...". Then, any "BEB" sequence demarcates entering and escaping a valley. Like in-cage rattle within a colloid, each valley represents a local meta-stable domain in the landscape where the system exhibits quasi-equilibrium behavior on time-scales shorter than the escape time.
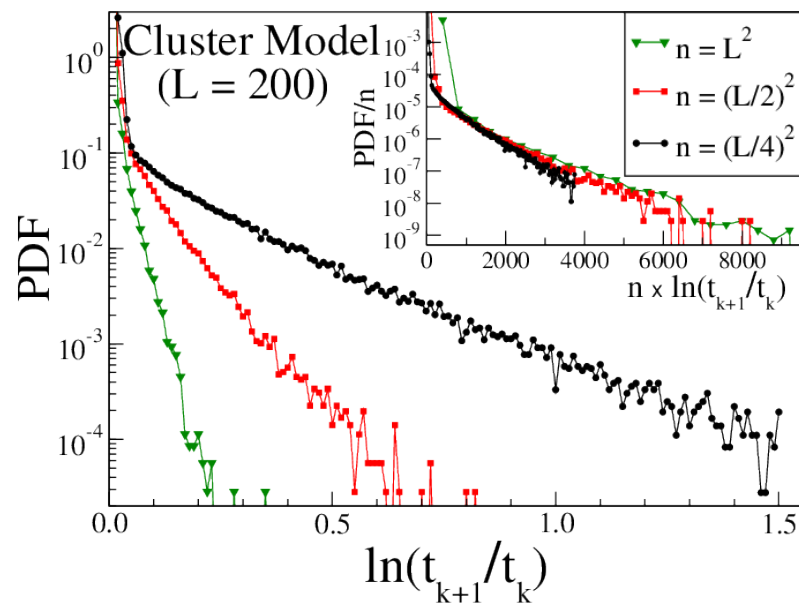
Figure 4.4: Log-Poisson statistics for the cluster model [150] on a square lattice of size $L = 100$. Inset: Data collapse when rescaled by n, as in Fig. 4.2b-c for colloid and spin glass.

Chapter 5

Localized vibrational modes in nonlinear networks

5.1 Introduction

In the previous chapters I have discussed the dynamics of glassy systems just beyond the glass transition. In this regime, materials are essentially solid, yet they evolve slowly through physical aging. Far beyond the glass transition, at nearly 0 K or at extremely high packing fraction, disordered solids can become so tightly bound to a local energy minimum that they can't undergo any rearrangements even on astronomical time scales [116, 196, 197]. Such a system is called 'jammed' [16, 111, 195, 198], or a low temperature glass. These systems can still exhibit vibrations around their local minimum, [14, 33] but the assortment of vibrational modes accessible to a disordered system is dramatically different than those available to a crystalline solid.

Every normal vibrational mode of a system has a natural frequency ω, and the

number of modes per unit frequency is called the density of states (DOS). The form of the density of states versus frequency determines the response of the system to thermal, optical, and acoustic inputs. The Debye model of crystalline solids calculates their density of states proportional to ω^2. This leads to a heat capacity which scales with the temperature as T^3. At low temperatures, heat transfer is mostly limited by scattering off these excitations, so the thermal conductivity follows the same trend. In low temperature glasses, the low frequency density of states is nearly constant due to a broad distribution of localized mode frequencies. This leads to a heat capacity which scales linearly with T, and the thermal conductivity as T^2 for $T < 1$K [47].

The established explanation of this discrepancy is that some of the low frequency modes in glasses are due to quantum tunneling [199–201]. The microscopic origin of these tunneling states is difficult to access [202], but the phenomena derived from this picture are consistent with most experimental data. Whatever structural features create these two-level tunneling states would make them strongly localized, so vibrational modes due to these states are decoupled from the plane wave modes in the Debye picture.

Evidence for this quantum mechanical picture is provided by experiments which apply acoustic pulses to a material and measure responses such as transmission, reflection, and absorption. The speed of sound has been found to depend on temperature. Some pulses are attenuated, but as the amplitude is increased the attenuation weakens [53, 59, 203, 204]. A sequence of pulses can cause a delayed 'echo' similar to those observed in magnetic resonance [59, 205]. These phenomena may all be explained using an ensemble of two-level tunneling states.

However, recent work has shown that some of these effects can be reproduced more accurately by a system of classical oscillators, if those oscillators are anharmonic and only weakly coupled [56, 133]. An ensemble of independent anharmonic oscillators can respond coherently to acoustic pulses [206–208]. If the oscillators are coupled, their nonlinearity causes them to exchange energy and thermalize instead. In glasses, structural disorder gives rise to localized normal modes at low frequencies [34]. Since these modes are spatially separated, excitations of a particular mode can't couple strongly to another mode. These naturally occurring localized modes are few and far between at the microscopic scale, but are numerous in even the smallest macroscopic sample. In Ref. [133], localized modes were studied in a simulated jammed packing of spheres. This method reproduced the 'phonon echo' phenomenon, but required averaging over thousands of systems. This difficulty arose due to the sparsity of localized modes in the randomly generated jammed system.

In order to demonstrate the nonlinear phenomena observed in experiments on low temperature glasses, our system must meet two requirements. 1) There must be a large number of localized modes forming an ensemble of anharmonic oscillators. 2) Those modes must absorb energy from acoustic pulses like those in experiments. In this chapter I present a system in which localized normal modes may be created deliberately at a higher density, allowing much higher computational efficiency. These manufactured defects may be interpreted as an abstraction of localized modes in a natural disordered material.

5.1.1 Normal mode calculation

The vibrational normal modes of a system can be calculated directly given an expression for the system's potential energy.

$$V(\mathbf{x}) = \sum_{i,j} V_{ij}(\mathbf{r_i}, \mathbf{r_j}) \tag{5.1}$$

Here $\mathbf{x}$ represents all of the degrees of freedom in a system, while $\mathbf{r_i}$ represents the position of particle i and V_{ij} is the pairwise potential between i and j. We chose to simulate a system in which the particles are constrained to move only in the z direction, so $\mathbf{r_i}$ is simply z_i. To compute the normal modes around a local minimum of V at a configuration $\mathbf{x_0}$ we compute the dynamical matrix $\mathbf{D}$, related to the Hessian of V

$$D_{ij} = \frac{1}{\sqrt{m_i m_j}} \frac{\partial^2 V}{\partial z_i \partial z_j}\Big|_{\mathbf{x}=\mathbf{x_0}} \tag{5.2}$$

Here m_i is the mass of particle i. Each of these second derivatives represent effective 'spring constants' between pairs of particles for low-amplitude oscillations. One can then find a set of linearly independent vibrational modes by calculating the eigenvectors of $\mathbf{D}$. Element i of such an eigenvector then corresponds to the amplitude with which particle i oscillates as part of that vibrational mode. Each of those modes has a natural frequency ω, and the eigenvalues of $\mathbf{D}$ correspond to ω^2

In general, if one applies a pulse with an arbitrary spatial distribution to a system, the oscillations of the system will evolve in a complex way. Since the normal modes are orthogonal, an excitation directly along one of these modes will simply oscillate sinusoidally indefinitely. That is, at least in the linear regime. Since disordered

systems have a rough energy landscape, the linear approximation can't hold forever. The oscillation frequency shifts quadratically with amplitude, and the energy begins to leak into modes of similar frequency.

A normal mode is 'localized' if a small fraction of the particles in the system have much larger amplitudes of oscillation in that mode than the rest of the particles do. Often there are two localized modes with similar frequencies, but with spatially separated sets of active particles. If one such mode is excited, even into the nonlinear regime, the input energy will be very slow to spread into the other mode.

To characterize the localization of normal modes, we calculate the participation ratio. Given an eigenmode $\mathbf{e}_k$, the participation ratio is

$$p(\mathbf{e}_k) = \frac{(\sum_i e_{ki}^2)^2}{N \sum_i e_{ki}^4}, \tag{5.3}$$

where e_{ki} is particle i's amplitude in the kth eigenmode. In a crystalline system, the normal modes are all plane waves, which yield the highest participation ratio of $\frac{2}{3}$. If the oscillation of a single particle dominates a mode, that mode would then have a participation ratio of $1/N$. Note that in a system with all boundaries either periodic or free, modes can exist with every other particle oscillating completely out of phase, yielding a participation ratio of 1.

A plot of participation ratio against frequency ω for each normal mode reveals ranges of frequencies populated by low-participation (localized) modes. In this chapter, I show that acoustic input in such a frequency range leads to localized normal modes oscillating independently even at high amplitudes. This ability to excite particular modes using generic pulses and have those modes retain that absorbed energy
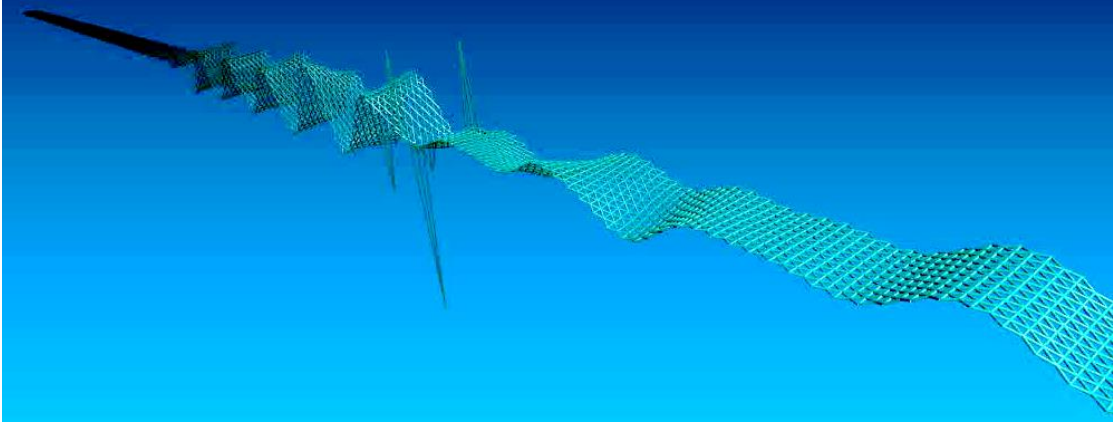
Figure 5.1: Here is a rendering demonstrating the structure and behavior of our system. Particles are arranged in a 2D triangular lattice, bonded to their neighbors (only the bonds are drawn here), then constrained to move only in the z direction. Acoustic pulses are generated by applying oscillatory forcing to the particles at one end of the system. As a pulse propagates across the system it interacts nonlinearly with 'defect' particles which have modified masses and bond properties.

is critical for a variety of nonlinear phenomena.

5.2 Simulation details

Simulations were carried out using the particle dynamics package HOOMD-blue [172, 173]. Contrary to the simulations presented in previous chapters, here the interaction potential between particles is attractive. Particle positions are initialized in the xy-plane, but then particles are constrained to only move in the z direction. This choice provides a variety of options for modifying and visualizing the system, while retaining the properties of wave propagation present in 3D experimental systems. See Figure 5.1 3D rendering of an acoustic pulse interacting with a few defects in our system.

The interaction between a pair of particles i and j which share a bond is a radially symmetric harmonic potential

$$V_{ij}(\mathbf{r_i}, \mathbf{r_j}) = \frac{k_{ij}}{2}(|\mathbf{r_i} - \mathbf{r_i}| - l_{ij})^2, \tag{5.4}$$

where k_{ij} is a spring constant and l_{ij} is a rest length for the ideal spring connecting i and j. All of the bonds are initially set with a rest length that is shorter than the xy distance between the particles. This ensures that the coplanar configuration is the ground state of the system $\mathbf{x_0}$.

The particles are initially arranged in a triangular lattice in a strip 9 particles wide and at least 108 particles long. These particular dimensions are chosen to ensure that periodic normal modes fit cleanly in the system at all frequencies. The elongation permits investigation of extremely long wavelength, low frequency modes with much lower computational cost than a fully 2D, or even 3D simulation. Trials were performed with various boundary conditions. For the results reported here, the narrow ends of the system were 'clamped' by initializing particles with infinite mass at the ends, and the long sides of the system have periodic boundary conditions.

The highest frequency behavior of this system is when two adjacent particles are oscillating perfectly out of phase. To ensure that all dynamics are captured faithfully, the simulation time step is set to one hundredth of this oscillation time scale. The simulations were carried out using HOOMD's built in NVE (Number, Volume, Energy conserving) integrator, which uses the Velocity-Verlet method [209]. More details of HOOMD and the computational properties of this system are discussed in Section 6.1.

5.2.1   Tuning nonlinearity

Though the pairwise potential used here is ideally harmonic, the fact that the particles are constrained to remain at distances greater than the rest length of the springs introduces anharmonicity. Writing Eqn. 5.4 in terms of the z-distance between particles gives

$$V_{ij}(\mathbf{r_i}, \mathbf{r_j}) = \frac{k_{i,j}}{2} \left(\sqrt{\Delta z^2 + s_{ij}^2} - l_{ij} \right)^2, \tag{5.5}$$

where s_{ij} is the fixed in-plane distance between i and j. Expanding this expression in terms of z and taking the second derivative gives

$$D_{i,j} = \frac{k_{ij}}{\sqrt{m_i m_j}} \left(1 - \frac{l_{ij}}{s_{ij}} + \frac{z^2 l_{ij}}{s_{ij}^3} \right) + O(z^4). \tag{5.6}$$

This form demonstrates several important facts. The potential is nonlinear. The pre-stretching of the bond creates an effective spring constant. If the rest length $l=0$, the effective spring constant is simply k. If $l = s$, the bond is 'relaxed' and the effective spring constant for low amplitude oscillations is 0. These facts provide tight control of the behavior of this system. There are also a couple of reasonability checks. If the rest length l is greater than the particle spacing s, then the effective spring constant is negative, which is not unreasonable considering that the system would buckle and destroy the assumed minimum energy configuration. When z is on the order of s, the nonlinear term begins to dominate, marking the breakdown of the linear approximation.

5.2.2 Tuning disorder

There are a variety of ways to introduce defects into this system to study nonlinear and localized normal modes. The masses of some particles m_i may be modified. The linear bond strength k and rest length l of any bond may be changed. Extremes of k are interesting, such as cutting bonds, or fusing particles to create a single mass with many bonds. The in-plane positions of particles can be shifted, affecting the inter-particle spacing. Any combination of these methods is viable. The properties of each of the 'normal' particles and bonds in the system are denoted $m_0 = 1, k_0 = 1, l_0 = 0, s_0 = 1$. The choice of $l_0 = 0$ for the majority of the system means that the medium should behave linearly except when pulses are tuned to interact with defects. Pulses should propagate without severe distortion, and the system should behave similarly at low and high amplitudes.

Further, one can choose exactly which particles or bonds are modified. In a natural or stochastically generated sample, the likelihood of forming a particular structural motif can be infinitesimal. Here one can construct a 'defect' which ignores linear oscillations, but produces strong localization at high amplitudes. Once such a design is discovered, it can be introduced to the system with whatever pattern or density is desired for study.

5.3 Vibrational modes

Once a system is constructed, vibrational normal modes are calculated using the linear terms in Eqn. 5.6. The spatial structure of each mode is readily visualized by
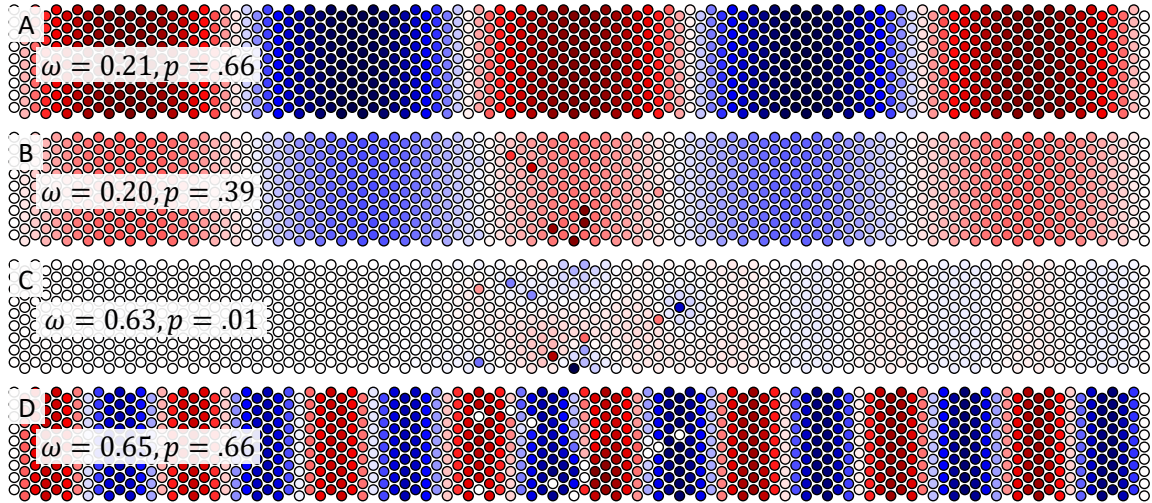
Figure 5.2: Here are representative examples of the variety of normal modes created. Here defect particles have $m = 10m_0$. Red coloring coresponds to positive displacements in the z-direction, and blue is negative. (A) Low frequency modes in a flawless system are plane waves. (B) Some plane wave modes exist even with defect sites, though the defects may have unusual amplitudes. (C) Massive particles create localized modes at particular frequencies. (D) Relaxed bonds at low amplitude don't participate in or dramatically distort modes.

coloring each particle according to its amplitude in the mode. A few such schematics are shown in Figure 5.2. In perfectly ordered systems, normal modes are simple plane waves. When a few particles are modified, some modes remain largely unchanged. Some modes, however, are distorted or even localized to just a few particles.

5.3.1 Localization

Making a single particle heavier creates a mode localized to that particle. If the mass of the defect particle is several times the mass of the regular particles m_0, that localized mode is at a frequency similar to the plane wave modes in a flawless system. Figure 5.3, shows that 'doping' the system with a few of these particles creates an
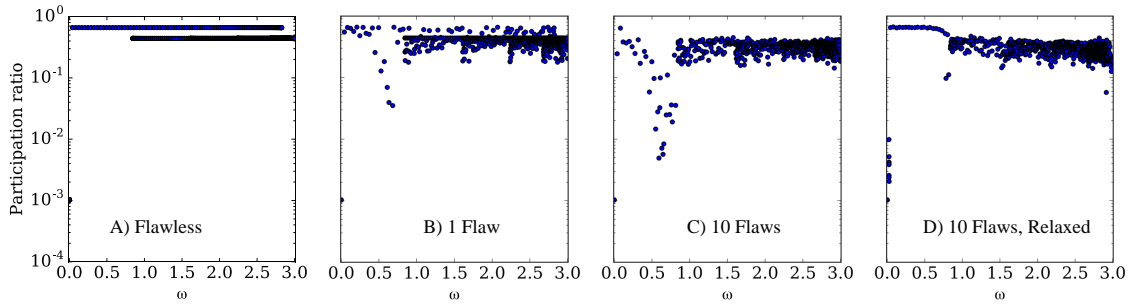
Figure 5.3: (A) Without defects, the participation ratios are clearly populated by plane waves with $p = 2/3$ or $4/9$ for 2D modes. Note the single low-participation point at $\omega = 0$ is due to the infinite-mass 'clamped' particles at the ends of the system. (B) A single particle with $m = 10m_0$ distorts most of the modes in the system, and particularly reduces p for a few modes around $\omega = .6$. (C) With 10 defects, few undistorted plane wave modes exist, and for a range of frequencies around $\omega = .6$ the regular modes are completely replaced by localized ones. (D) By relaxing the bonds on the defect sites to $l = .999$, their interaction with the rest of the system at low amplitude is reduced and the plane wave modes are recovered.

assortment of localized modes of similar frequencies and suppresses the plane wave modes in this frequency range.

5.3.2 Amplitude dependence

To even lay the groundwork for reproducing the nonlinear acoustic phenomena discussed in Section 5.1, we must leverage the nonlinearity in Eqn. 5.6. To demonstrate this we construct a system which responds differently to low and high amplitude pulses. We can anticipate the behavior of the system by considering distinct sets of vibrational modes with low and high amplitudes. As discussed in Section 5.2.1, if $l = 0$ the low and high amplitude behavior of a bond is the same. If $l = s$, the bond is very weak at low amplitude and becomes stronger with larger oscillations.

We found that a few weakly bonded particles were one of the least disruptive

types of defects, as shown in Figures 5.2 D and 5.3 D. By introducing defects with 'relaxed' bonds with $l = s$ instead of $k = 0$, the low frequency, low amplitude normal modes are similar to those of a flawless system. However, with increasing amplitude, the more massive particles begin to interact with the system and create modes that look like those in Figures 5.2 C and 5.3 C.

5.4 Excitation Pulses

In Ref. [133], 'phonon echoes' were observed by applying pulses as a sinusoidal standing wave throughout the system. In experiments on low temperature glasses, pulses are applied and measured using acoustic transducers on the surface of a sample. In an effort to more closely emulate experiment, here we apply forcing to the particles on one end of the system in the form of a gaussian wave packet, which then propagates across the system, interacting with defects along the way.

Figure 5.4 shows the propagation of an input pulse across the system and its interaction with defects at low and high amplitudes. At low amplitudes the pulse may momentarily appear to localize, but quickly rolls over the defects and continues as a mildly deformed packet. At high amplitude, the pulse is more reflected than transmitted through the doped region, due to the interaction with extra-massive particles. Further, the pulse is more dramatically reshaped, and the defect particles continue to oscillate in a localized mode long after the pulse would have passed them over.
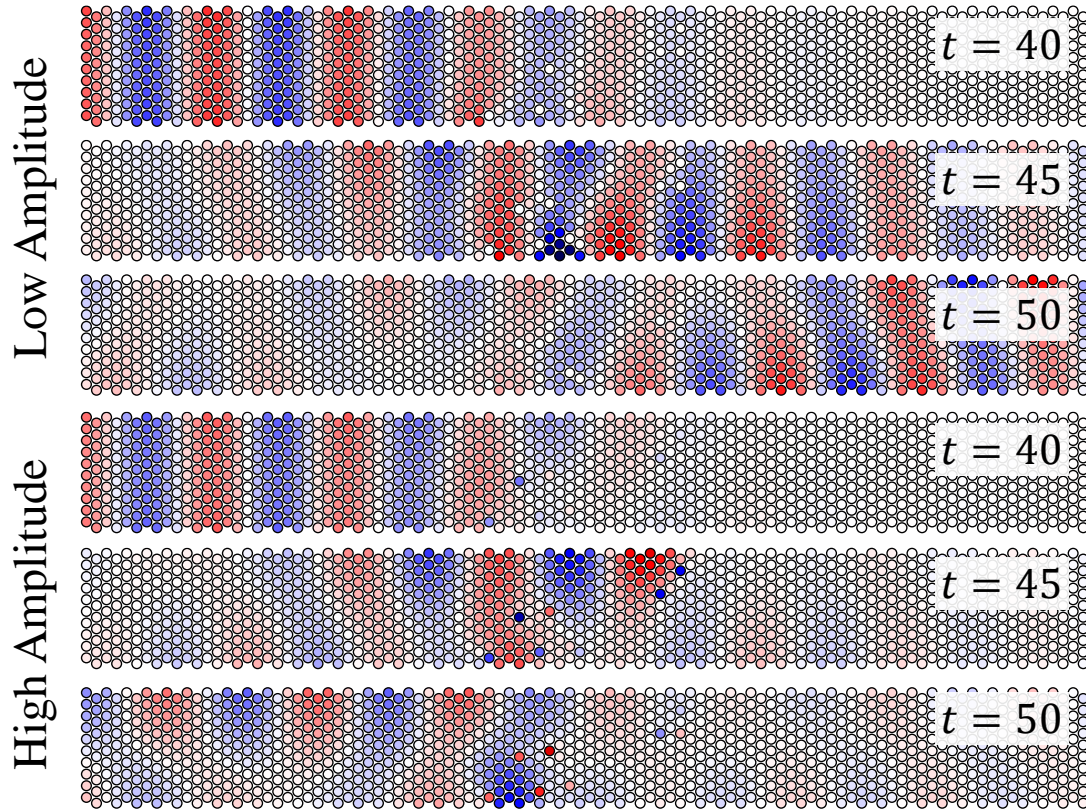
Figure 5.4: Propagation of acoustic pulses across a system with a cluster of defects. There are 10 defect particles with $m = 10m_0$ and $l = .999$. The system and pulse shape are identical, but the pulse amplitude is 100 times larger in the second time series. The color scheme is rescaled accordingly. The pulse is a gaussian wave packet with two cycles per σ, cut off at 5σ. The shown particles are the middle 100 columns out of a system 1000 columns wide.

5.4.1 Resonant absorption

To show that energy is absorbed from a plane-wave-like pulse by a localized mode, we observe the kinetic energy. Figure 5.5 shows a plot of kinetic energy vs. time and x-coordinate averaged over a half-cycle and over y-coordinates. In a system without defects, the pulse simply bounces back and forth between the clamped boundaries. A low amplitude pulse scatters mildly off defects. A high amplitude pulse deposits
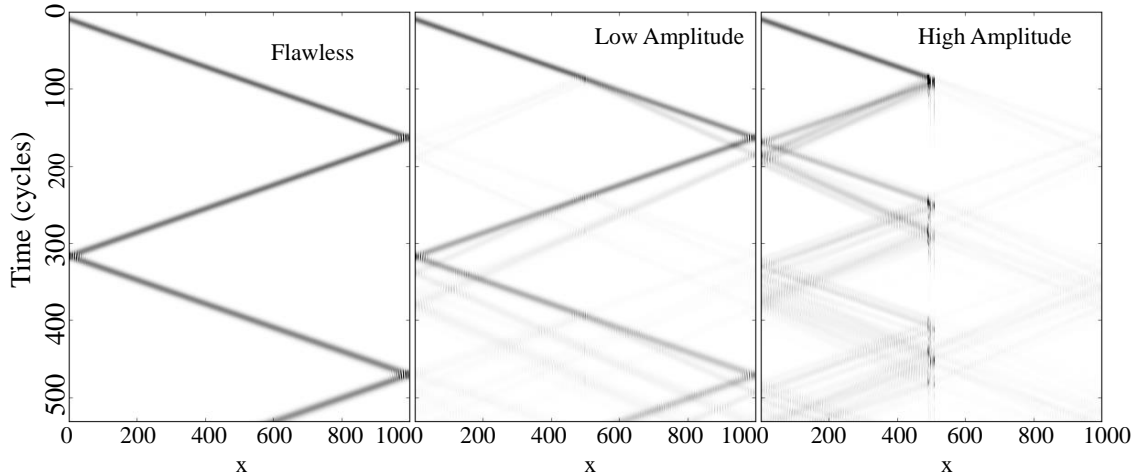
Figure 5.5: Resonant absorption of kinetic energy from a wave packet by localized modes. Intensity corresponds to the kinetic energy of a column of particles averaged over half of an input pulse cycle. Displayed intensity is scaled with the peak amplitude of the input pulse. The system and pulses are the same as in Figure 5.4.

a significant amount of energy in the localized modes created by the defects. This behavior is reliant on the frequency of the input pulse matching that of the localized modes, so that the modes can resonate with the pulse.

The streaks in Figure 5.5 at the defect sites show that the localized modes continue to oscillate for dozens of cycles after the pulse retreats. A broader pulse containing more high amplitude cycles can drive the localized modes to even higher amplitudes. However, these modes are nonlinearly coupled to the rest of the system, so they do eventually decay as energy leaks into other modes. Further this decay will speed up as the amplitude of the localized modes are driven higher. This decay is slowed, though, but the strong localization, and may be improved with further tuning.

5.5 Conclusions

In this chapter, I have described a system of nonlinearly coupled masses, into which defects are easily placed to create localized normal modes. These deliberately placed localized modes are intended as an abstraction of the localized modes which arise naturally in a disordered solid. Since localized modes are weakly coupled to each other and the plane wave modes in a system, they can behave as independent oscillators. Such an ensemble of anharmonic oscillators would account for a number of nonlinear acoustic phenomena observed in low temperature glasses.

This work is merely the foundation for investigation of these acoustic phenomena. One immediate question is how quickly the energy in a mode decays as a function of its amplitude. Also important is the fraction of energy absorbed from a pulse as the pulse amplitude increases. If a large set of modes can be excited for an extended period of time, we should be able to reproduce the phonon echo effect in a single instance of the system. We can also study phenomena like the speed of sound and pulse attenuation, and how they depend on frequency, amplitude, and the density of defect sites.

There is a growing field of mechanical metamaterials which functionalize nonlinear effects [210–212]. Some efforts have also been made recently to construct disordered materials with targeted functional properties [213]. These disordered mechanisms are generally more robust to defects or damage, and can implement multifunctionality. With better understanding of the nonlinear mechanical properties of disordered systems there may be opportunities to develop novel robust functional materials.

Chapter 6

Computational methods

6.1 Particle dynamics

Particle dynamics simulations essentially aim to solve Newton's equations of motion given a set of N objects and the interaction potentials ϕ_{ij} between them. Since these potentials depend on the positions of the particles $\mathbf{r}_i$ which can evolve chaotically, there is no analytical solution, and the equations of motion must be integrated numerically. Usually this is accomplished with the Velocity-Verlet method [209], which computes the position and velocity of particle i at time $t = \Delta t$ from those values at $t = 0$ using

$$\mathbf{x}_i(\Delta t) = \mathbf{x}_i(0) + \mathbf{v}_i(0)\Delta t + \mathbf{F}_i(0)\frac{\Delta t^2}{2m_i} \tag{6.1}$$

$$\mathbf{v}_i(\Delta t) = \mathbf{v}_i(0) + [\mathbf{F}_i(0) + \mathbf{F}_i(\Delta t)]\frac{\Delta t}{2m_i} \tag{6.2}$$

$$\mathbf{F}_i(t) = \nabla\Phi_i(t) \tag{6.3}$$

$$\Phi_i(t) = \sum_{j\neq i} \phi_{ij}(\mathbf{r}_i(t), \mathbf{r}_j(t)), \tag{6.4}$$

6.1.1 Interactions

Eqn. 6.4 makes it obvious that the computationally intensive part of this process is the calculation of the potential, which makes each time step an $O(N^2)$ operation. If the interaction is weak at long range, it is usual to only compute the interaction for particles within some cutoff radius of each other. However, there is some evidence that such a cutoff can destroy certain physical phenomena [214]. Further, to implement a cutoff, one must still compute the distances between particles, which is in principle still $O(N^2)$. Tree-based algorithms using a bounding volume hierarchy can reduce this to $O(N)$ [215], but the choice of cutoff distance and neighbor list update frequency still have significant impact on performance.

The choice in Chapters 3 and 4 to study a system approximating hard spheres is highly optimal for reducing the complexity of interaction calculations. The harmonic potential is easy to compute, and this potential and its derivative fall continuously to zero at the cutoff, which avoids inaccuracies due to discontinuous forces [216]. The restriction of interaction to overlapping particles puts a clear cutoff radius at one particle diameter.

The list of 'neighboring' particles which could interact can be updated either periodically, or triggered by the movement of a particle beyond a certain threshold. Due to the confined dynamics which are the focus of Chapters 2,3, and 4, particles rarely rearrange, so the triggered update is very efficient. As the rearrangement events become rarer, the neighbor updates naturally adapt.

In Chapter 5 we chose to simulate strictly constrained particles and permanently bonded interactions in part to avoid this complication of updating neighbor lists. The manipulation of bond strength and particle offsets described in Section 5.2.1 allowed us to simulate a nontrivial anharmonic system with a relatively cheap potential.

6.1.2 GPU Acceleration

Though there are many calculations to perform in Eqns. 6.1 - 6.4, they are trivially parallel. Further, in most cases, these equations can be reduced to kernels which perform the exact same operations on each particle or pair of particles. This situation is ripe for GPU acceleration.

HOOMD-Blue is a particle dynamics package for python which is designed to scale from a single CPU to thousands of GPUs [172, 173]. The simulations in Chapters 3,4, and 5 were carried out using HOOMD-Blue on a Tesla K-40 GPU, which has 2880 CUDA cores. This massive parallelization allowed us to simulate 100,000 particles over 10^7 time steps in a day in a desktop environment.

There is one small caveat with this technique. GPU computing libraries do not offer the user control of the order in which operations are carried out. Since floating point arithmetic is not strictly commutative, combining the vast number of updates

throughout a simulation can in general have a variety of results. These deviations are generally very small, but since many-body interactions are chaotic the detailed trajectories from these parallelized simulations are not technically reproducible [217]. The trajectories obtained are still valid, and results from averaging over many trajectories are reproducible. Nevertheless, this is an important point to note.

6.1.3 Time Step

Though the particle updates within an integration step are largely parallelizable, integration through time is serial. The number of time steps is then a less forgiving restriction on a simulation's scale. Humans naturally observe phenomena that occur over a time scale of seconds. In contrast, collisions between atoms in a dense material occur over femtoseconds. Since running simulations for 10^{15} time steps is not generally practical, compromises must be made. Either a simulation is coarse-grained such that short time dynamics are averaged out, or the simulation runs short and hopes that experimentally observed phenomena persist to shorter time scales. The dynamical simulations in this thesis have taken the latter approach, which places clear constraints on their time steps and durations.

In the simulations of physical aging in Chapters 3 and 4, the fastest phenomenon which must be captured is the collision of two particles. The next important duration is the time between consecutive collisions. Recall as well that we were investigating intermittent rearrangement events. In order for a rearrangement to be observed there must be some notion of a 'cage', which can only be defined through multiple collisions, creating another time scale. Finally, in order to test our hypothesis about

the decreasing event rate, data must be collected over multiple orders of magnitude in time, the bottom end of which may be the rearrangement time.

This brings us to an unfortunate result of our choice of potential. The distance that particles interpenetrate during a collision is roughly a factor of 100 smaller than the distance traveled between collisions. Accurately simulating those collisions then requires multiple integration steps during the collision. Adding a decade for a cage to be determined, then adding three more to collect useful data makes the simulation span 10^7 time steps. This is computationally feasible, but a 100,000 particle simulation took approximately 20 hours to run on our single GPU with 2000 cores. Results discussed in previous chapters were then averaged over 10 runs. Since the particle interactions are short range and neighbor list updates are rare, so this system would likely scale well to multiple GPUs.

In the vibrational mode simulations discussed in Chapter 5, dynamical time scales are well described by the oscillation frequencies of the modes under study. The shortest relevant time scale is set by the highest frequency modes in the system, the Debye frequency. In the specific work presented in Chapter 5, excitations were studied at roughly a fifth of the Debye frequency. Acoustic pulses must then be at least a few oscillation cycles long, and we need at least another order of magnitude in time to observe the propagation of such a pulse. Spanning these time scales then only requires 10^5 time steps. This project was also only simulating 10,000 particles, so each simulation only takes a few minutes.

However, the simulations in Chapter 5 represent only the groundwork for simulations more similar to real glasses. In Ref. [133], thousands of localized modes were

necessary to observe an acoustic echo. Including that many defects in a single instance would require a system at least ten times larger. Further, the localized modes in low temperature glasses discussed in Section 5.1 are many orders of magnitude below the Debye frequency. These effects combined would put these simulations in the days-long regime as well.

6.1.4 Other methods

A different method for studying disordered many-body systems which should be mentioned is hard particle Monte Carlo simulation [218]. HPMC simulations update a system by generating random small trial displacements of particles and checking if the new configuration would be allowed. If it is not, the move is rejected, otherwise it is carried out. HPMC is popular for its theoretical accessibility [219–221]and computational simplicity (particularly in higher dimensions [222–224]).

An adaptation of the HPMC method is called 'swap Monte Carlo' [225], in which as well as small displacements, trial moves may involve swapping the locations of two particles of different sizes. This method can equilibrate systems far below the glass transition, providing insight into the equilibrium phase transitions [66, 226, 227] and material properties [111] in disordered solids. However, the non-equilibrium process of physical aging is important in experiment and applications as discussed in Section 1.2. The unphysical equilibration mechanism in swap MC wipes out the aging process.

6.2   Cluster Model

The cluster model of aging colloids is mentioned in Chapters 2, 3, and 4 and Ref. [149, 150]. This is a coarse-grained model in which particles fill all sites in a square lattice. The only movement particles can undergo is to swap positions with a neighboring particle. These swaps are meant to represent the rearrangements in a colloidal system. Here the in-cage rattle motion is ignored.

Each particle in the system belongs to a cluster, and at initialization each particle has its own cluster, as in Figure 6.1A. In each update step, each particle in a cluster of size $h = 1$ swaps position with a random neighbor, and that neighbor's cluster expands to cover both sites. Particles in a cluster of size $h > 1$ do not initiate swaps. In this manner, after one time step, the entire system is frozen into clusters of a few particles.

However, a cluster with $h > 1$ can break into h single-particle clusters with probability $P(h) = exp(-h)$. Those free particles then begin swapping into the remaining clusters. As the simulation progresses, larger clusters begin to form, reducing the rate of breakup events. When a large cluster breaks, particles may either join an adjacent (probably also large) cluster, or form new small clusters (see Figure 6.1E). Those small clusters are then exponentially more likely to break sooner than the surrounding larger clusters. The inevitable outcome of a large cluster breaking is then for its particles to diffuse into the surrounding large clusters (Figure 6.1F). This decreases the number of clusters by one and marginally increases the average cluster size. This flurry of localized activity re-creates the phenomenon of dynamical heterogeneity discussed in Section 1.3 and observed in many detailed spin glass and colloidal
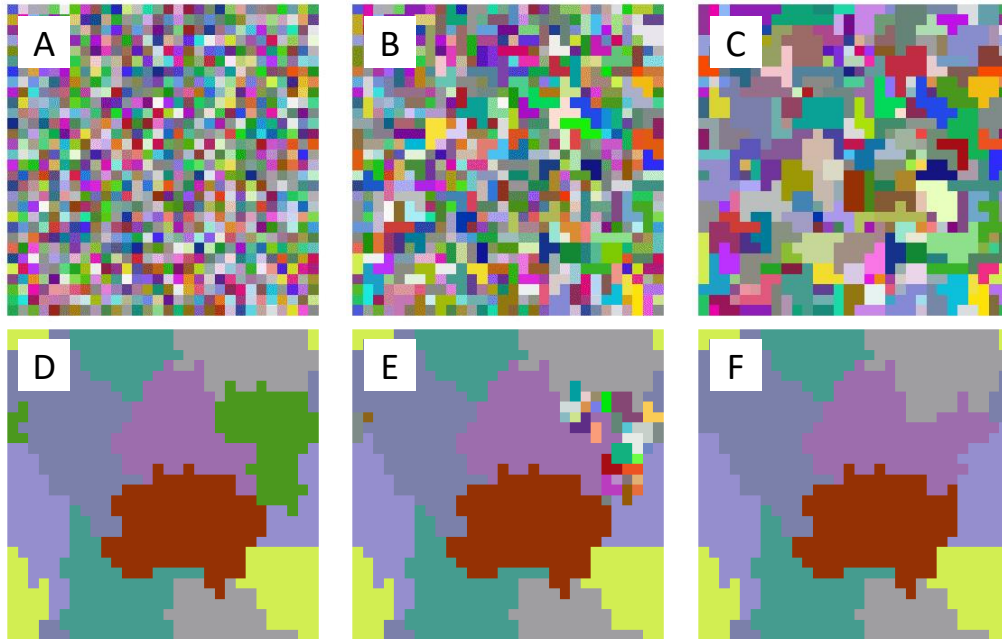
Figure 6.1: The growth and breakup dynamics of the cluster model. A) Initialization to singleton clusters. B) Small clusters which break up quickly. C) Slow aggregation of larger clusters. D) Eventual dominance of a few large clusters. E) Large cluster breaks up. F) remnants of large breakup quickly assimilate to neighboring clusters.

experiments and simulations [31, 113, 190, 228–232].

Generating random numbers to compare to $P(h)$ for each cluster in each time step is inefficient since $P(h)$ is very small and most breakup attempts are rejected. We can instead exploit the fact that survival times for a cluster of size h are exponentially distributed through time. Instead of drawing many numbers from a uniform distribution, we can draw one number from that exponential distribution and wait until that time to break the cluster. This approach is called the 'waiting time method' [85]. Once the times for breakups are determined, the simulation time can jump to the next scheduled event. This allows us to simulate very rare events efficiently.

Chapter 7

Summary

In this thesis I have presented a variety of simulated systems intended to study structural and dynamical phenomena in disordered solids. In the introductory chapter I laid out the context for the work I carried out and the connections between the various phenomena encountered. Disordered solids are ubiquitous in nature and manufactured materials, yet the principles governing their behavior are still being unfolded.

In this thesis I have focused on the phenomena of localized dynamics in disordered solids. In particular the bulk of this material is devoted to the non-equilibrium relaxation process of physical aging. Aging presents a problem in manufacturing due to the slow change in material properties and their dependence on environmental conditions. The appearance of similar phenomena in a variety of dissimilar systems (polymers, grains, foams, spins, ...) presents a fascinating challenge in physics as well. The framework of record dynamics attempts to unify these disparate systems by focusing on generic features of rough energy landscapes. Exploration of such

a landscape is then limited by thermal fluctuations or spontaneous cooperation of independent degrees of freedom.

In Chapter 2 I analyzed data from a quasi-2D colloidal experiment, and found the evolution of dynamics to correspond well to the record dynamics prediction. I also measured a dynamical correlation length which increased as the system aged, consistent with the idea that more wide-spread cooperation is necessary for continued relaxation as the system ages.

In Chapter 3 I developed particle dynamics simulations to emulate and extend the experimental data. With larger samples I was able to resolve details of particle displacement statistics for very rare rearrangement events. I distinguished rearrangements from in-cage rattle by pinpointing the first moment any pair of particles become neighbors. This metric demonstrated clearly that the event rate decays inversely with the age of the system. Further I showed that the entire distribution of single-particle displacements evolves in lock-step with the number of these rearrangements that have occurred.

In Chapter 4 I considered the inter-event times and found they form a Poisson process under a logarithmic parameterization of time. This analysis discriminates between the history-dependent dynamics of record-breaking fluctuations and a merely decelerating process such as a random walk through independent traps. This chapter also compared results directly between colloidal and spin glass simulations, which indicates the generality of these results. Recall that spin glasses are representative of a broad class of complex systems through the problem of constraint satisfaction.

In Chapter 5 I developed a system of masses connected by nonlinear springs to

study vibrational modes in disordered solids. By introducing particles with specific properties I created localized vibrational modes analogous to the soft spots observed in jammed systems. I demonstrated that these localized modes can resonantly absorb energy from acoustic inputs, and their localization prevents that energy from thermalizing quickly. This compact system of anharmonic localized modes serves as a framework for future studies of nonlinear acoustic phenomena in disordered systems.

In Chapter 6 I described in detail the computational techniques which made these projects possible. Understanding of both the physical and computational principles at play allowed me to create novel simulations which capture known phenomena, produce new information, and are computationally efficient.

In conclusion, I will remark one last time that the phenomena discussed in this thesis: structural disorder, frustrated constraints, complex optimization landscapes, and intermittent and localized activity, these are all phenomena which affect systems from the molecules in a plastic cup to the interaction of animal species on the global stage. Pushing forward on our understanding of these phenomena will improve both our practical capacity to improve our lives and our understanding of the world around us.

Bibliography

[1] J. C. Phillips and R. Kerner, Structure and function of window glass and Pyrex, *J. Chem. Phys.*, **128**, 174506 (2008).

[2] V. I. Kasatochkin and B. V. Lukin, The Molecular Structure and Properties of Rubber, *Rubber Chem. Technol.*, **25**, 12–14 (1952).

[3] C. Buckley, Glass-rubber constitutive model for amorphous polymers near the glass transition, *Polymer (Guildf).*, **36**, 3301–3312 (1995).

[4] S. Danesi and R. S. Porter, Blends of isotactic polypropylene and ethylene-propylene rubbers: rheology, morphology and mechanics, *Polymer (Guildf).*, **19**, 448–457 (1978).

[5] D. N. Theodorou and U. W. Suter, Detailed molecular structure of a vinyl polymer glass, *Macromolecules*, **18**, 1467–1478 (1985).

[6] R. A. Hayes, The relationship between glass temperature, molar cohesion, and polymer structure, *J. Appl. Polym. Sci.*, **5**, 318–321 (1961).

[7] M. J. Dejneka, The luminescence and structure of novel transparent oxyfluoride glass-ceramics, *J. Non. Cryst. Solids*, **239**, 149–155 (1998).

[8] F. Graner, B. Dollet, C. Raufaste, and P. Marmottant, Discrete rearranging disordered patterns, part I: Robust statistical tools in two or three dimensions, *Eur. Phys. J. E*, **25**, 349–369 (2008).

[9] D. Bi, X. Yang, M. C. Marchetti, and M. L. Manning, Motility-Driven Glass and Jamming Transitions in Biological Tissues, *Phys. Rev. X*, **6**, 021011 (2016).

[10] L. McNally, E. Bernardy, J. Thomas, A. Kalziqi, J. Pentz, S. P. Brown, B. K. Hammer, P. J. Yunker, and W. C. Ratcliff, Killing by Type VI secretion drives genetic phase separation and correlates with increased cooperation, *Nat. Commun.*, **8**, 14371 (2017).

[11] A. NIKOLAIDIS and T. P. LABUZA, Glass Transition State Diagram of a Baked Cracker and Its Relationship to Gluten, *J. Food Sci.*, **61**, 803–806 (1996).

[12] H. Gloria and D. Sievert, Changes in the Physical State of Sucrose during Dark Chocolate Processing, *J. Agric. Food Chem.*, **49**, 2433–2436 (2001).

[13] P. Chaudhuri, L. Berthier, and S. Sastry, Jamming transitions in amorphous packings of frictionless spheres occur over a continuous range of volume fractions, *Phys. Rev. Lett.*, **104**, 1–4 (2010).

[14] Q. Wu, T. Bertrand, M. D. Shattuck, and C. S. O'Hern, Response of jammed packings to thermal fluctuations, *Phys. Rev. E*, **96**, 062902 (2017).

[15] J. C. Burton, P. Y. Lu, and S. R. Nagel, Energy loss at propagating jamming fronts in granular gas clusters, *Phys. Rev. Lett.*, **111**, 188001 (2013).

[16] T. S. Majmudar, M. Sperl, S. Luding, and R. P. Behringer, Jamming Transition in Granular Systems, *Phys. Rev. Lett.*, **98**, 058001 (2007).

[17] J. B. KNIGHT, C. G. FANDRICH, C. N. LAU, H. M. JAEGER, and S. R. NAGEL, Density relaxation in a vibration granular material, *Phys. Rev. E*, **51** (1995).

[18] L. Berthier, G. Biroli, J. P. Bouchaud, L. Cipelletti, and W. van Saarloos, *Dynamical Heterogeneities in Glasses, Colloids, and Granular Media* (OUP Oxford) (2011), ISBN 9780191729799.

[19] A. M. Kraynik, Foam Structure: From Soap Froth to Solid Foams, *MRS Bull.*, **28**, 275–278 (2003).

[20] L. Cipelletti and L. Ramos, Slow dynamics in glasses, gels and foams, *Curr. Opin. Colloid Interface Sci.*, **7**, 228–234 (2002).

[21] R. Blumenfeld, Stress transmission in planar disordered solid foams, *J. Phys. A. Math. Gen.*, **36**, 2399–2411 (2003).

[22] J. Kwak, H.-H. Jo, T. Luttinen, and I. Kosonen, Jamming transitions induced by an attraction in pedestrian flow, *Phys. Rev. E*, **96**, 022319 (2017).

[23] M. Muramatsu and T. Nagatani, Jamming transition in two-dimensional pedestrian traffic, *Phys. A Stat. Mech. its Appl.*, **275**, 281–291 (2000).

[24] P. G. Debenedetti and F. H. Stillinger, Supercooled liquids and the glass transition, *Nature*, **410**, 259–267 (2001).

[25] T. Jonsson, J. Mattsson, C. Djurberg, F. A. Khan, P. Nordblad, and P. Svedlindh, Aging in a Magnetic Particle System, *Phys. Rev. Lett.*, **75**, 4138–4141 (1995).

[26] E. Vincent, J. P. Bouchaud, D. S. Dean, and J. Hammann, Aging in spin glasses as a random walk: Effect of a magnetic field, *Phys. Rev. B*, **52**, 1050–1060 (1995).

[27] F. N. Kelley and F. Bueche, Viscosity and glass temperature relations for polymer-diluent systems, *J. Polym. Sci.*, **50**, 549–556 (1961).

[28] E. R. Weeks and D. a. Weitz, Subdiffusion and the cage effect studied near the colloidal glass transition, *Chem. Phys.*, **284**, 361–367 (2001).

[29] D. E. Masri, M. Pierno, L. Berthier, and L. Cipelletti, Ageing and ultra-slow equilibration in concentrated colloidal hard spheres, *J. Phys. Condens. Matter*, **17**, S3543–S3549 (2005).

[30] P. Yunker, Z. Zhang, K. B. Aptowicz, and a. G. Yodh, Irreversible rearrangements, correlated domains, and local structure in aging glasses, *Phys. Rev. Lett.*, **103**, 1–4 (2009).

[31] R. Candelier, O. Dauchot, and G. Biroli, Building blocks of dynamical heterogeneities in dense granular media, *Phys. Rev. Lett.*, **102**, 1–4 (2009).

[32] O. Dauchot, G. Marty, and G. Biroli, Dynamical heterogeneity close to the jamming transition in a sheared granular material, *Phys. Rev. Lett.*, **95**, 1–4 (2005).

[33] C. Brito, O. Dauchot, J.-p. Bouchaud, G. Biroli, and J.-p. Bouchaud, Elementary excitation modes in a granular glass above jamming, *Soft Matter*, **6**, 3013–3022 (2010).

[34] A. J. Liu and S. R. Nagel, The Jamming Transition and the Marginally Jammed Solid, *Annu. Rev. Condens. Matter Phys.*, **1**, 347–369 (2010).

[35] S. Deshmukh and D. Bharambe, Synthesis of polymeric pour point depressants for Nada crude oil (Gujarat, India) and its impact on oil rheology, *Fuel Process. Technol.*, **89**, 227–233 (2008).

[36] I. Masalova, A. Malkin, P. Slatter, and K. Wilson, The rheological characterization and pipeline flow of high concentration water-in-oil emulsions, *J. Nonnewton. Fluid Mech.*, **112**, 101–114 (2003).

[37] H. SUNDARAM, B. VOIGTS, K. BEER, and M. MELAND, Comparison of the Rheological Properties of Viscosity and Elasticity in Two Categories of Soft Tissue Fillers: Calcium Hydroxylapatite and Hyaluronic Acid, *Dermatologic Surg.*, **36**, 1859–1865 (2010).

[38] A.-M. Ionescu, M. Alaminos, J. d. l. C. Cardona, J. d. D. García-López Durán, M. González-Andrades, R. Ghinea, A. Campos, E. Hita, and M. d. M. Pérez, Investigating a novel nanostructured fibrin–agarose biomaterial for human cornea tissue engineering: Rheological properties, *J. Mech. Behav. Biomed. Mater.*, **4**, 1963–1973 (2011).

[39] I. Sumita and M. Manga, Suspension rheology under oscillatory shear and its geophysical implications, *Earth Planet. Sci. Lett.*, **269**, 468–477 (2008).

[40] R. D. Andrus and K. H. Stokoe II, Liquefaction Resistance of Soils from Shear-Wave Velocity, *J. Geotech. Geoenvironmental Eng.*, **126**, 1015–1025 (2000).

[41] U. Strom, J. Hendrickson, R. Wagner, and P. Taylor, Disorder-induced far infrared absorption in amorphous materials, *Solid State Commun.*, **15**, 1871–1875 (1974).

[42] L. Schertel, I. Wimmer, P. Besirske, C. M. Aegerter, G. Maret, S. Polarz, and G. J. Aubry, Tunable high-index photonic glasses, *Phys. Rev. Mater.*, **3**, 015203 (2019).

[43] Y. Kawakami and T. Sugisaka, Relationships between structure, permeability and glass transition temperature of oligodimethylsiloxanyl substituted polymers, *J. Memb. Sci.*, **50**, 189–205 (1990).

[44] S. C. George and S. Thomas, Transport phenomena through polymeric systems, *Prog. Polym. Sci.*, **26**, 985–1017 (2001).

[45] K. E. Thompson and H. S. Fogler, Modeling flow in disordered packed beds from pore-scale fluid mechanics, *AIChE J.*, **43**, 1377–1389 (1997).

[46] G. Cheng, A. Yu, and P. Zulli, Evaluation of effective thermal conductivity from the structure of a packed bed, *Chem. Eng. Sci.*, **54**, 4199–4209 (1999).

[47] R. C. Zeller and R. O. Pohl, Thermal Conductivity and Specific Heat of Non-crystalline Solids, *Phys. Rev. B*, **4**, 2029–2041 (1971).

[48] J. Clerc, G. Giraud, J. Laugier, and J. Luck, The electrical conductivity of binary disordered systems, percolation clusters, fractals and related models, *Adv. Phys.*, **39**, 191–309 (1990).

[49] D. Adler, L. P. Flora, and S. D. Senturia, Electrical conductivity in disordered systems, *Solid State Commun.*, **12**, 9–12 (1973).

[50] J. Bernasconi, Electrical Conductivity in Disordered Systems, *Phys. Rev. B*, **7**, 2252–2260 (1973).

[51] S. Suzuki, N. Shibutani, K. Mimura, M. Isshiki, and Y. Waseda, Improvement in strength and electrical conductivity of Cu–Ni–Si alloys by aging and cold rolling, *J. Alloys Compd.*, **417**, 116–120 (2006).

[52] M. J. Starink and X. M. Li, A model for the electrical conductivity of peak-aged and overaged Al-Zn-Mg-Cu alloys, *Metall. Mater. Trans. A*, **34**, 899–911 (2003).

[53] S. Hunklinger, W. Arnold, S. Stein, R. Nava, and K. Dransfeld, Saturation of the ultrasonic absorption in vitreous silica at low temperatures, *Phys. Lett. A*, **42**, 253–255 (1972).

[54] C. Enss and S. Hunklinger, Incoherent Tunneling in Glasses at Very Low Temperatures, *Phys. Rev. Lett.*, **79**, 2831–2834 (1997).

[55] J. Classen, T. Burkert, C. Enss, and S. Hunklinger, in Beyond the tunneling model—Elastic properties of vitreous silica at low temperaturespages 279–291 (Springer Berlin Heidelberg, Berlin, Heidelberg).

[56] D. C. Vural and A. J. Leggett, Universal sound absorption in amorphous solids: A theory of elastically coupled generic blocks, *J. Non. Cryst. Solids*, **357**, 3528–3537 (2011).

[57] B. Golding, J. E. Graebner, B. I. Halperin, and R. J. Schutz, Nonlinear Phonon Propagation in Fused Silica below 1 K, *Phys. Rev. Lett.*, **30**, 223–226 (1973).

[58] W. Arnold, C. Martinon, and S. Hunklinger, DIRECT EXPERIMENTAL OB-SERVATION OF SPECTRAL DIFFUSION IN VITREOUS SILICA AT LOW TEMPERATURES, *Le J. Phys. Colloq.*, **39**, C6–961–C6–962 (1978).

[59] J. L. Black and B. I. Halperin, Spectral diffusion, phonon echoes, and saturation recovery in glasses at low temperatures, *Phys. Rev. B*, **16**, 2879–2895 (1977).

[60] J. Vannimenus and G. Toulouse, Theory of the frustration effect. II. Ising spins on a square lattice, *J. Phys. C Solid State Phys.*, **10**, L537–L542 (1977).

[61] M. Mézard and G. Parisi, Statistical physics of structural glasses, *J. Phys. Condens. Matter*, **12**, 6655–6673 (2000).

[62] N. Iikawa, M. M. Bandi, and H. Katsuragi, Force-chain evolution in a two-dimensional granular packing compacted by vertical tappings, *Phys. Rev. E*, **97**, 032901 (2018).

[63] E. Ben-Naim, J. Knight, E. Nowak, H. Jaeger, and S. Nagel, Slow relaxation in granular compaction, *Phys. D*, **123**, 380–385 (1998).

[64] E. R. Nowak, J. B. Knight, E. Ben-Naim, H. M. Jaeger, and S. R. Nagel,

Density Fluctuations In Vibrated Granular Materials, *Phys. Rev. E*, **57**, 1971–1982 (1998).

[65] C. Brito and M. Wyart, Heterogeneous dynamics, marginal stability and soft modes in hard sphere glasses, *J. Stat. Mech. Theory Exp.*, **2007**, L08003–L08003 (2007).

[66] C. Scalliet, L. Berthier, and F. Zamponi, Absence of Marginal Stability in a Structural Glass, *Phys. Rev. Lett.*, **119**, 205501 (2017).

[67] F. Krzakala, A. Montanari, F. Ricci-Tersenghi, G. Semerjian, and L. Zdeborova, Gibbs states and the set of solutions of random constraint satisfaction problems, *Proc. Natl. Acad. Sci.*, **104**, 10318–10323 (2007).

[68] S. Boettcher and A. G. Percus, Optimization with extremal dynamics, *Complexity*, **8**, 57–62 (2002).

[69] S. Kirkpatrick, C. D. Gelatt, and M. P. Vecchi, Optimization by Simulated Annealing, *Science (80-.).*, **220**, 671–680 (1983).

[70] G. Tarjus, S. A. Kivelson, Z. Nussinov, and P. Viot, The frustration-based approach of supercooled liquids and the glass transition: a review and critical assessment, *J. Phys. Condens. Matter*, **17**, R1143–R1182 (2005).

[71] H. Tanaka, A simple physical model of liquid - glass transition: intrinsic fluctuating interactions and random fields hidden in glass-forming liquids, *J. Phys. Condens. Matter*, **10**, L207–L214 (1998).

[72] S. A. Cook, in The complexity of theorem-proving procedurespages 151–158 (ACM Press, New York, New York, USA) (1971).

[73] D. Sherrington and S. Kirkpatrick, Solvable Model of a Spin-Glass, *Phys. Rev. Lett.*, **35**, 1792–1796 (1975).

[74] K. Jonason, E. Vincent, J. Hammann, J. P. Bouchaud, and P. Nordblad, Memory and Chaos Effects in Spin Glasses, *Phys. Rev. Lett.*, **81**, 3243 (1998).

[75] P. Nordblad, P. Svedlindh, L. Lundgren, and L. Sandlund, Time decay of the remanent magnetization in a CuMn spin glass, *Phys. Rev. B*, **33**, 645 (1986).

[76] V. S. Zotev, G. F. Rodriguez, G. G. Kenning, R. Orbach, E. Vincent, and J. Hammann, Role of initial conditions in spin-glass aging experiments, *Phys. Rev. B*, **67**, 184422 (2003).

[77] L. Lundgren, P. Svedlindh, P. Nordblad, and O. Beckman, Dynamics of the Relaxation-Time Spectrum in a CuMn Spin-Glass, *Phys. Rev. Lett.*, **51**, 911–914 (1983).

[78] E. Vincent, J. Hammann, M. Ocio, J.-P. Bouchaud, and L. F. Cugliandolo, in Slow dynamics and aging in spin glassespages 184–219 (Springer Berlin Heidelberg) (1997).

[79] P. T. Dumitrescu, R. Vasseur, and A. C. Potter, Logarithmically Slow Relaxation in Quasiperiodically Driven Random Spin Chains, *Phys. Rev. Lett.*, **120**, 070602 (2018).

[80] L. A. Fernandez, V. Martin-Mayor, G. Parisi, and B. Seoane, Temperature chaos in 3D Ising spin glasses is driven by rare events, *Europhys. Lett.*, **103**, 67003 (2013).

[81] K. H. Fischer and J. A. Hertz, *Spin glasses* (Cambridge University Press, Cambridge) (1991), ISBN 9780511628771.

[82] M. Mezard, G. Parisi, and M. Virasoro, *Spin Glass Theory and Beyond*, volume 9 of *World Scientific Lecture Notes in Physics* (WORLD SCIENTIFIC) (1986), ISBN 978-9971-5-0116-7.

[83] T. Castellani and A. Cavagna, Spin-glass theory for pedestrians, *J. Stat. Mech. Theory Exp.*, **2005**, P05012 (2005).

[84] M. Baity-Jesi, G. Biroli, and C. Cammarota, Activated aging dynamics and effective trap model description in the random energy model, *J. Stat. Mech. Theory Exp.*, **2018**, 013301 (2018).

[85] J. Dall and P. Sibani, Faster Monte Carlo Simulations at Low Temperatures. The Waiting Time Method, *Comput. Phys. Commun.*, **141**, 1–14 (2001).

[86] P. Sibani and J. Dall, Log-Poisson statistics and full aging in glassy systems, *Europhys. Lett.*, **64**, 8–14 (2003).

[87] P. Sibani and H. J. Jensen, Intermittency, aging and extremal fluctuations, *Europhys. Lett.*, **69**, 563–569 (2005).

[88] A. Amir, Y. Oreg, and Y. Imry, On relaxations and aging of various glasses, *Proc. Natl. Acad. Sci.*, **109**, 1850–1855 (2012).

[89] R. D. Priestley, Structural Relaxation of Polymer Glasses at Surfaces, Interfaces, and In Between, *Science (80-.).*, **309**, 456–459 (2005).

[90] J. Zhao, S. L. Simon, and G. B. McKenna, Using 20-million-year-old amber to test the super-Arrhenius behaviour of glass-forming systems, *Nat. Commun.*, **4**, 1783 (2013).

[91] Y. Huang and D. Paul, Physical aging of thin glassy polymer films monitored by gas permeability, *Polymer (Guildf).*, **45**, 8377–8393 (2004).

[92] C. Reed and S. Cichanowskil, The fundamentals of aging in HV polymer-film capacitors, *IEEE Trans. Dielectr. Electr. Insul.*, **1**, 904–922 (1994).

[93] M. Henkel, M. Pleimling, and R. Sanctuary, editors, *Ageing and the Glass Transition*, volume 716 of *Lecture Notes in Physics* (Springer Berlin Heidelberg, Berlin, Heidelberg) (2007), ISBN 978-3-540-69683-4.

[94] S. Sastry, P. G. Debenedetti, and F. H. Stillinger, Signatures of distinct dynamical regimes in the energy landscape of a glass-forming liquid, *Nature*, **393**, 554–557 (1998).

[95] K. Broderix, K. K. Bhattacharya, A. Cavagna, A. Zippelius, and I. Giardina, Energy landscape of a lennard-jones liquid: statistics of stationary points., *Phys. Rev. Lett.*, **85**, 5360–3 (2000).

[96] F. Sicard, Computing transition rates for rare events: When Kramers theory meets the free-energy landscape, *Phys. Rev. E*, **98**, 052408 (2018).

[97] L. Angelani, R. Di Leonardo, G. Ruocco, A. Scala, and F. Sciortino, Saddles in the Energy Landscape Probed by Supercooled Liquids, *Phys. Rev. Lett.*, **85**, 5356–5359 (2000).

[98] A. F. Voter, A method for accelerating the molecular dynamics simulation of infrequent events, *J. Chem. Phys.*, **106**, 4665–4677 (1997).

[99] J. Dall and P. Sibani, Exploring Valleys of Aging Systems: The Spin Glass Case, *Eur. Phys. J. B*, **36**, 233–243 (2003).

[100] K. V. Edmond, C. R. Nugent, and E. R. Weeks, Influence of confinement on dynamical heterogeneities in dense colloidal samples, *Phys. Rev. E*, **85**, 041401 (2012).

[101] Z. Zhang, P. J. Yunker, P. Habdas, and A. G. Yodh, Cooperative Rearrangement Regions and Dynamical Heterogeneities in Colloidal Glasses with Attractive Versus Repulsive Interactions, *Phys. Rev. Lett.*, **107**, 208303 (2011).

[102] C. Toninelli, M. Wyart, L. Berthier, G. Biroli, and J. P. Bouchaud, Dynamical susceptibility of glass formers: Contrasting the predictions of theoretical scenarios, *Phys. Rev. E*, **71**, 1–20 (2005).

[103] E. Vidal Russell and N. E. Israeloff, Direct observation of molecular cooperativity near the glass transition, *Nature*, **408**, 695–698 (2000).

[104] E. Donth, The size of cooperatively rearranging regions at the glass transition, *J. Non. Cryst. Solids*, **53**, 325–330 (1982).

[105] G. Adam and J. H. Gibbs, On the Temperature Dependence of Cooperative Relaxation Properties in Glass-Forming Liquids, *J. Chem. Phys.*, **43**, 139–146 (1965).

[106] J. D. Stevenson, J. Schmalian, and P. G. Wolynes, The shapes of cooperatively rearranging regions in glass-forming liquids, *Nat. Phys.*, **2**, 268–274 (2006).

[107] L.-N. Zou and S. R. Nagel, Glassy Dynamics in Thermally Activated List Sorting, *Phys. Rev. Lett.*, **104**, 257201 (2010).

[108] E. Pitard, Finite-size effects and intermittency in a simple aging system, *Phys. Rev. E*, **71**, 041504 (2005).

[109] J. P. Bouchaud and G. Biroli, On the Adam-Gibbs-Kirkpatrick-Thirumalai-Wolynes scenario for the viscosity increase in glasses, *J. Chem. Phys.*, **121**, 7347–7354 (2004).

[110] K. Vollmayr-Lee, Single particle jumps in a binary Lennard-Jones system below the glass transition, *J. Chem. Phys.*, **121**, 4781–4794 (2004).

[111] Y. Jin, P. Urbani, F. Zamponi, and H. Yoshino, A stability-reversibility map unifies elasticity, plasticity, yielding, and jamming in hard sphere glasses, *Sci. Adv.*, **4**, eaat6387 (2018).

[112] X. Du and E. R. Weeks, Energy barriers, entropy barriers, and non-Arrhenius behavior in a minimal glassy model, *Phys. Rev. E*, **93**, 062613 (2016).

[113] E. R. Weeks, J. C. Crocker, A. C. Levitt, A. Schofield, and D. a. Weitz, Three-

Dimensional Direct Imaging of Structural Relaxation Near the Colloidal Glass Transition, *Science (80-.).*, **287**, 627–631 (2000).

[114] M. Maier, A. Zippelius, and M. Fuchs, Emergence of long-ranged stress correlations at the liquid to glass transition, *Phys. Rev. Lett.*, **119**, 1–5 (2017).

[115] C. Zhang, N. Gnan, T. G. Mason, E. Zaccarelli, and F. Scheffold, Dynamical and structural signatures of the glass transition in emulsions, *J. Stat. Mech. Theory Exp.*, **2016**, 094003 (2016).

[116] P. Chaudhuri, L. Berthier, and W. Kob, Universal nature of particle displacements close to glass and jamming transitions, *Phys. Rev. Lett.*, **99**, 2–5 (2007).

[117] R. M. Ernst, S. R. Nagel, and G. S. Grest, Search for a correlation length in a simulation of the glass transition, *Phys. Rev. B*, **43**, 8070–8080 (1991).

[118] P. Yunker, Z. Zhang, and a. G. Yodh, Observation of the disorder-induced crystal-to-glass transition, *Phys. Rev. Lett.*, **104**, 2–5 (2010).

[119] K. Watanabe and H. Tanaka, Direct Observation of Medium-Range Crystalline Order in Granular Liquids Near the Glass Transition, *Phys. Rev. Lett.*, **100**, 158002 (2008).

[120] W. Mickel, S. C. Kapfer, G. E. Schröder-Turk, and K. Mecke, Shortcomings of the bond orientational order parameters for the analysis of disordered particulate matter, *J. Chem. Phys.*, **138**, 044501 (2013).

[121] Y. T. Shen, T. H. Kim, a. K. Gangopadhyay, and K. F. Kelton, Icosahedral Order, Frustration, and the Glass Transition: Evidence from Time-Dependent

Nucleation and Supercooled Liquid Structure Studies, *Phys. Rev. Lett.*, **102**, 057801 (2009).

[122] C. Dasgupta, A. V. Indrani, S. Ramaswamy, and M. K. Phani, Is There a Growing Correlation Length near the Glass Transition?, *Europhys. Lett.*, **15**, 307–312 (1991).

[123] S. S. Schoenholz, E. D. Cubuk, E. Kaxiras, and A. J. Liu, Relationship between local structure and relaxation in out-of-equilibrium glassy systems, *Proc. Natl. Acad. Sci.*, **114**, 263–267 (2017).

[124] M. Harrington, A. J. Liu, and D. J. Durian, Machine learning characterization of structural defects in amorphous packings of dimers and ellipses, *Phys. Rev. E*, **99**, 022903 (2019).

[125] X. Ma, Z. S. Davidson, T. Still, R. J. S. Ivancic, S. S. Schoenholz, A. J. Liu, and A. G. Yodh, Heterogeneous Activation, Local Structure, and Softness in Supercooled Colloidal Liquids, *Phys. Rev. Lett.*, **122**, 028001 (2019).

[126] T. A. Sharp, S. L. Thomas, E. D. Cubuk, S. S. Schoenholz, D. J. Srolovitz, and A. J. Liu, Machine learning determination of atomic dynamics at grain boundaries, *Proc. Natl. Acad. Sci.*, **115**, 10943–10947 (2018).

[127] M. S. G. Razul, G. S. Matharoo, and P. H. Poole, Spatial correlation of the dynamic propensity of a glass-forming liquid, *J. Phys. Condens. Matter*, **23**, 235103 (2011).

[128] A. Cavagna, I. Giardina, and G. Parisi, Analytic Computation of the Instantaneous Normal Modes Spectrum in Low-Density Liquids, *Phys. Rev. Lett.*, **83**, 108–111 (1999).

[129] M. L. Manning and A. J. Liu, Vibrational modes identify soft spots in a sheared disordered packing, *Phys. Rev. Lett.*, **107**, 108302 (2010).

[130] M. Ozawa, A. Ikeda, K. Miyazaki, and W. Kob, Ideal Glass States Are Not Purely Vibrational: Insight from Randomly Pinned Glasses, *Phys. Rev. Lett.*, **121**, 205501 (2018).

[131] J. Zylberg, E. Lerner, Y. Bar-Sinai, and E. Bouchbinder, Local thermal energy as a structural indicator in glasses, *Proc. Natl. Acad. Sci.*, **114**, 7289–7294 (2017).

[132] E. Lerner, G. Düring, and E. Bouchbinder, Statistics and Properties of Low-Frequency Vibrational Modes in Structural Glasses, *Phys. Rev. Lett.*, **117**, 1–5 (2016).

[133] J. C. Burton and S. R. Nagel, Echoes from anharmonic normal modes in model glasses, *Phys. Rev. E*, **93**, 032905 (2016).

[134] L. Buisson, L. Bellon, and S. Ciliberto, Intermittency in ageing, *J. Phys. Condens. Matter*, **15**, S1163–S1179 (2003).

[135] L. Buisson, S. Ciliberto, and A. Garcimartín, Intermittent origin of the large violations of the fluctuation-dissipation relations in an aging polymer glass, *Europhys. Lett.*, **63**, 603–609 (2003).

[136] H. Bissig, S. Romer, L. Cipelletti, V. Trappe, and P. Schurtenberger, Intermittent dynamics and hyper-aging in dense colloidal gelsThis paper was originally presented as a poster at the Faraday Discussion 123 meeting., *Phys. Chem. Commun.*, **6**, 21–23 (2003).

[137] T. Kajiya, T. Narita, V. Schmitt, F. Lequeux, and L. Talini, Slow dynamics and intermittent quakes in soft glassy systems, *Soft Matter*, **9**, 11129 (2013).

[138] R. Zargar, B. Nienhuis, P. Schall, and D. Bonn, Direct Measurement of the Free Energy of Aging Hard Sphere Colloidal Glasses, *Phys. Rev. Lett.*, **110**, 258301 (2013).

[139] A. Crisanti and F. Ritort, Intermittency of glassy relaxation and the emergence of a non-equilibrium spontaneous measure in the aging regime, *Europhys. Lett.*, **66**, 253–259 (2004).

[140] P. Sibani, Aging and intermittency in a p-spin model of a glass, *Phys. Rev. E*, **74**, 1–6 (2006).

[141] P. Sibani, G. F. Rodriguez, and G. G. Kenning, Intermittent quakes and record dynamics in the thermoremanent magnetization of a spin-glass, *Phys. Rev. B*, **74**, 1–6 (2006).

[142] L. Oliveira, H. Jensen, M. Nicodemi, and P. Sibani, Record dynamics and the observed temperature plateau in the magnetic creep-rate of type-II superconductors, *Phys. Rev. B*, **71**, 1–7 (2005).

[143] G. F. Rodriguez, G. G. Kenning, and R. Orbach, Full Aging in Spin Glasses, *Phys. Rev. Lett.*, **91**, 1–4 (2003).

[144] G. F. Rodriguez, G. G. Kenning, and R. Orbach, Effect of the thermal quench on aging in spin glasses, *Phys. Rev. B*, **88**, 054302 (2013).

[145] T. O. Richardson, E. J. H. Robinson, K. Christensen, H. J. Jensen, N. R. Franks, and A. B. Sendova-Franks, Record Dynamics in Ants, *PLoS One*, **5**, e9621 (2010).

[146] A. Parsaeian and H. E. Castillo, Growth of spatial correlations in the aging of a simple structural glass, *Phys. Rev. E*, **78**, 060105 (2008).

[147] K. Vollmayr-Lee, C. H. Gorman, and H. E. Castillo, Universal scaling in the aging of the strong glass former SiO2, *J. Chem. Phys.*, **144**, 234510 (2016).

[148] R. E. Courtland and E. R. Weeks, Direct visualization of aging in colloidal glasses, *J. Phys. Condens. Matter*, **15**, S359–S365 (2002).

[149] S. Boettcher and P. Sibani, Ageing in dense colloids as diffusion in the logarithm of time, *J. Phys. Condens. Matter*, **23**, 065103 (2011).

[150] N. Becker, P. Sibani, S. Boettcher, and S. Vivek, Mesoscopic model of temporal and spatial heterogeneity in aging colloids, *J. Phys. Condens. Matter*, **26**, 505102 (2014).

[151] P. Sibani and K. H. Hoffmann, Hierarchical models for aging and relaxation of spin glasses, *Phys. Rev. Lett.*, **63**, 2853–2856 (1989).

[152] P. Sibani, Coarse-graining complex dynamics: Continuous Time Random Walks vs. Record Dynamics, *Europhys. Lett.*, **101**, 30004 (2013).

[153] F. H. Stillinger and T. A. Weber, Packing Structures and Transitions in Liquids and Solids, *Science (80-.)*., **225**, 983–989 (1984).

[154] F. H. Stillinger, Exponential multiplicity of inherent structures, *Phys. Rev. E*, **59**, 48–51 (1999).

[155] G. L. Hunter and E. R. Weeks, The physics of the colloidal glass transition, *Reports Prog. Phys.*, **75**, 066501 (2012).

[156] P. Anderson, H. J. Jensen, L. P. Oliveira, and P. Sibani, Evolution in complex systems, *Complexity*, **10**, 8 (2004).

[157] F. Ritort, Glassiness in a Model without Energy Barriers, *Phys. Rev. Lett.*, **75**, 1190–1193 (1995).

[158] P. Sibani and S. Boettcher, Record dynamics in the parking-lot model, *Phys. Rev. E*, **93**, 062141 (2016).

[159] P. L. Krapivsky and E. Ben-Naim, Collective properties of adsorption–desorption processes, *J. Chem. Phys.*, **100**, 6778–6782 (1994).

[160] C. Tang, K. Wiesenfeld, P. Bak, S. Coppersmith, and P. Littlewood, Phase organization, *Phys. Rev. Lett.*, **58**, 1161–1164 (1987).

[161] A. J. Bray and M. A. Moore, Metastable states in spin glasses with short-ranged interactions, *J. Phys. C*, **14**, 1313–1327 (1981).

[162] A. Heuer, Exploring the potential energy landscape of glass-forming systems: from inherent structures via metabasins to macroscopic transport, *J. Phys. Condens. Matter*, **20**, 373101 (2008).

[163] P. Sibani, J. C. Schön, P. Salamon, and J.-O. Andersson, Emergent Hierarchical Structures in Complex-System Dynamics, *Europhys. Lett.*, **22**, 479–485 (1993).

[164] S. Boettcher and P. Sibani, Comparing extremal and thermal explorations of energy landscapes, *Eur. Phys. J. B*, **44**, 317–326 (2005).

[165] P. Sibani and P. B. Littlewood, Slow dynamics from noise adaptation, *Phys. Rev. Lett.*, **71**, 1482–1485 (1993).

[166] D. El Masri, L. Berthier, and L. Cipelletti, Subdiffusion and intermittent dynamic fluctuations in the aging regime of concentrated hard spheres, *Phys. Rev. E*, **82**, 1–11 (2010).

[167] L. Berthier, G. Biroli, J.-P. Bouchaud, L. Cipelletti, D. E. Masri, D. L'Hôte, F. Ladieu, and M. Pierno, Direct Experimental Evidence of a Growing Length Scale Accompanying the Glass Transition, *Science (80-.).*, **310**, 1797–1800 (2005).

[168] L. Berthier, Dynamic Heterogeneity in Amorphous Materials, *Physics (College. Park. Md).*, **4**, 42 (2011).

[169] C. Maggi, R. Di Leonardo, G. Ruocco, and J. C. Dyre, Measurement of the Four-Point Susceptibility of an Out-of-Equilibrium Colloidal Solution of Nanopar-

ticles Using Time-Resolved Light Scattering, *Phys. Rev. Lett.*, **109**, 097401 (2012).

[170] T. Yanagishima, J. Russo, and H. Tanaka, Common mechanism of thermodynamic and mechanical origin for ageing and crystallization of glasses, *Nat. Commun.*, **8**, 1–10 (2017).

[171] K. Binder and W. Kob, *Glassy Materials and Disordered Solids* (WORLD SCIENTIFIC) (2005), ISBN 978-981-256-510-5.

[172] J. A. Anderson, C. D. Lorenz, and A. Travesset, General purpose molecular dynamics simulations fully implemented on graphics processing units, *J. Comput. Phys.*, **227**, 5342–5359 (2008).

[173] J. Glaser, T. D. Nguyen, J. A. Anderson, P. Lui, F. Spiga, J. A. Millan, D. C. Morse, and S. C. Glotzer, Strong scaling of general-purpose molecular dynamics simulations on GPUs, *Comput. Phys. Commun.*, **192**, 97–107 (2015).

[174] D. M. Robe, S. Boettcher, P. Sibani, and P. Yunker, Record Dynamics: Direct Experimental Evidence from Jammed Colloids, *Europhys. Lett.*, **116**, 38003 (2016).

[175] R. Colin, A. M. Alsayed, J.-C. Castaing, R. Goyal, L. Hough, and B. Abou, Spatially heterogeneous dynamics in a thermosensitive soft suspension before and after the glass transition, *Soft Matter*, **7**, 4504 (2011).

[176] C. H. Rycroft, VORO++: A three-dimensional Voronoi cell library in C++, *Chaos*, **19** (2009).

[177] A. J. Archer, P. Hopkins, and M. Schmidt, Dynamics in inhomogeneous liquids and glasses via the test particle limit, *Phys. Rev. E*, **75**, 040501 (2007).

[178] D. A. Stariolo and G. Fabricius, Fickian crossover and length scales from two point functions in supercooled liquids, *J. Chem. Phys.*, **125**, 064505 (2006).

[179] S. Boettcher, D. M. Robe, and P. Sibani, Aging is a log-Poisson process, not a renewal process, *Phys. Rev. E*, **98**, 020602 (2018).

[180] J. P. Bouchaud, Weak ergodicity breaking and aging in disordered systems, *J. Phys. I*, **2**, 1705–1713 (1992).

[181] S. Burov, R. Metzler, and E. Barkai, Aging and nonergodicity beyond the Khinchin theorem, *Proc. Natl. Acad. Sci.*, **107**, 13228–13233 (2010).

[182] J. H. P. Schulz, E. Barkai, and R. Metzler, Aging Renewal Theory and Application to Random Walks, *Phys. Rev. X*, **4**, 011028 (2014).

[183] R. Metzler, J.-H. Jeon, A. G. Cherstvy, and E. Barkai, Anomalous diffusion models and their properties: non-stationarity, non-ergodicity, and ageing at the centenary of single particle tracking, *Phys. Chem. Chem. Phys.*, **16**, 24128–24164 (2014).

[184] R. Metzler, Forever ageing, *Nat. Phys.*, **12**, 113–114 (2016).

[185] M. Warren and J. Rottler, Quench, Equilibration, and Subaging in Structural Glasses, *Phys. Rev. Lett.*, **110**, 025501 (2013).

[186] P. Sibani and G. G. Kenning, Origin of end-of-aging and subaging scaling behavior in glassy dynamics, *Phys. Rev. E*, **81**, 011108 (2010).

[187] A. G. Cherstvy, D. Vinod, E. Aghion, A. V. Chechkin, and R. Metzler, Time averaging, ageing and delay analysis of financial time series, *New J. Phys.*, **19**, 063045 (2017).

[188] X. Hu, L. Hong, M. Dean Smith, T. Neusius, X. Cheng, and J. C. Smith, The dynamics of single protein molecules is non-equilibrium and self-similar over thirteen decades in time, *Nat. Phys.*, **12**, 171–174 (2016).

[189] X. Brokmann, J.-P. Hermier, G. Messin, P. Desbiolles, J.-P. Bouchaud, and M. Dahan, Statistical aging and nonergodicity in the fluorescence of single nanocrystals., *Phys. Rev. Lett.*, **90**, 120601 (2003).

[190] P. Sibani and S. Boettcher, Mesoscopic real-space structures in spin-glass aging: The Edwards-Anderson model, *Phys. Rev. B*, **98**, 054202 (2018).

[191] M. A. Lomholt, L. Lizana, R. Metzler, and T. Ambjörnsson, Microscopic Origin of the Logarithmic Time Evolution of Aging Processes in Complex Systems, *Phys. Rev. Lett.*, **110**, 208301 (2013).

[192] Y. Lahini, O. Gottesman, A. Amir, and S. M. Rubinstein, Nonmonotonic Aging and Memory Retention in Disordered Mechanical Systems, *Phys. Rev. Lett.*, **118**, 085501 (2017).

[193] L. F. Cugliandolo and J. Kurchan, Analytical solution of the off-equilibrium dynamics of a long-range spin-glass model, *Phys. Rev. Lett.*, **71**, 173–176 (1993).

[194] V. Lubchenko and P. G. Wolynes, Theory of aging in structural glasses, *J. Chem. Phys.*, **121**, 2852–2865 (2004).

[195] V. Lubchenko and P. G. Wolynes, Aging, Jamming, and the Limits of Stability of Amorphous Solids, *J. Phys. Chem. B*, **122**, 3280–3295 (2018).

[196] P. Ballesta, A. Duri, and L. Cipelletti, Unexpected drop of dynamical heterogeneities in colloidal suspensions approaching the jamming transition, *Nat. Phys.*, **4**, 550–554 (2008).

[197] C. S. O'Hern, L. E. Silbert, A. J. Liu, and S. R. Nagel, Jamming at zero temperature and zero applied stress: The epitome of disorder, *Phys. Rev. E*, **68**, 011306 (2003).

[198] M. Muramatsu, T. Irie, and T. Nagatani, Jamming transition in pedestrian counter flow, *Phys. A Stat. Mech. its Appl.*, **267**, 487–498 (1999).

[199] P. w. Anderson, B. I. Halperin, and c. M. Varma, Anomalous low-temperature thermal properties of glasses and spin glasses, *Philos. Mag.*, **25**, 1–9 (1972).

[200] W. A. Phillips, Tunneling states in amorphous solids, *J. Low Temp. Phys.*, **7**, 351–360 (1972).

[201] W. A. Phillips, Two-level states in glasses, *Reports Prog. Phys.*, **50**, 1657–1708 (1987).

[202] A. J. Leggett and D. C. Vural, "Tunneling Two-Level Systems" Model of the Low-Temperature Properties of Glasses: Are "Smoking-Gun" Tests Possible?, *J. Phys. Chem. B*, **117**, 12966–12971 (2013).

[203] W. Arnold, S. Hunklinger, S. Stein, and K. Dransfeld, Nonlinear ultrasonic attenuation in glasses, *J. Non. Cryst. Solids*, **14**, 192–200 (1974).

[204] J. E. Graebner, L. C. Allen, B. Golding, and A. B. Kane, Acoustic saturation in a glass at low temperatures, *Phys. Rev. B*, **27**, 3697–3708 (1983).

[205] B. Golding and J. E. Graebner, Phonon Echoes in Glass, *Phys. Rev. Lett.*, **37**, 852–855 (1976).

[206] W. Kegel and R. Gould, On the theory of pulse stimulated radiation from a plasma, *Phys. Lett.*, **19**, 531–532 (1965).

[207] G. F. Herrmann, R. M. Hill, and D. E. Kaplan, Cyclotron Echoes in Plasmas, *Phys. Rev.*, **156**, 118–133 (1967).

[208] K. Fossheim, K. Kajimura, T. G. Kazyaka, R. L. Melcher, and N. S. Shiren, Dynamic polarization echoes in piezoelectric powders, *Phys. Rev. B*, **17**, 964–998 (1978).

[209] G. J. Martyna, D. J. Tobias, and M. L. Klein, Constant pressure molecular dynamics algorithms, *J. Chem. Phys.*, **101**, 4177–4189 (1994).

[210] N. P. Mitchell, L. M. Nash, D. Hexner, A. M. Turner, and W. T. M. Irvine, Amorphous topological insulators constructed from random point sets, *Nat. Phys.*, **14**, 380–385 (2018).

[211] S. Alagoz and B. Baykant Alagoz, Sonic crystal acoustic switch device, *J. Acoust. Soc. Am.*, **133**, EL485–EL490 (2013).

[212] N. Boechler, G. Theocharis, and C. Daraio, Bifurcation-based acoustic switching and rectification, *Nat. Mater.*, **10**, 665–668 (2011).

[213] J. W. Rocks, H. Ronellenfitsch, A. J. Liu, S. R. Nagel, and E. Katifori, Limits of multifunctionality in tunable networks, *Proc. Natl. Acad. Sci.*, **116**, 2506–2511 (2019).

[214] J. E. Pye, C. E. Wood, and J. C. Burton, Precursors to Molecular Slip on Smooth Hydrophobic Surfaces (2018).

[215] M. P. Howard, J. A. Anderson, A. Nikoubashman, S. C. Glotzer, and A. Z. Panagiotopoulos, Efficient neighbor list calculation for molecular simulation of colloidal systems using graphics processing units, *Comput. Phys. Commun.*, **203**, 45–52 (2016).

[216] S. Toxvaerd and J. C. Dyre, Communication: Shifted forces in molecular dynamics, *J. Chem. Phys.*, **134**, 081102 (2011).

[217] M. Crane, Questionable Answers in Question Answering Research: Reproducibility and Variability of Published Results, *Trans. Assoc. Comput. Linguist.*, **6**, 241–252 (2018).

[218] K. Binder, editor, *Monte Carlo Methods in Statistical Physics*, volume 7 of *Topics in Current Physics* (Springer Berlin Heidelberg, Berlin, Heidelberg) (1986), ISBN 978-3-540-16514-9.

[219] J. Kurchan, G. Parisi, and F. Zamponi, Exact theory of dense amorphous hard spheres in high dimension I. The free energy, *J. Stat. Mech. Theory Exp.*, **2012**, P10012 (2012).

[220] J. Kurchan, G. Parisi, P. Urbani, and F. Zamponi, Exact Theory of Dense

Amorphous Hard Spheres in High Dimension. II. The High Density Regime and the Gardner Transition, *J. Phys. Chem. B*, **117**, 12979–12994 (2013).

[221] P. Charbonneau, J. Kurchan, G. Parisi, P. Urbani, and F. Zamponi, Exact theory of dense amorphous hard spheres in high dimension. III. The full replica symmetry breaking solution, *J. Stat. Mech. Theory Exp.*, **2014**, P10009 (2014).

[222] J. a. van Meel, B. Charbonneau, A. Fortini, and P. Charbonneau, Hard-sphere crystallization gets rarer with increasing dimension, *Phys. Rev. E*, **80**, 061110 (2009).

[223] J. A. van Meel, D. Frenkel, and P. Charbonneau, Geometrical frustration: A study of four-dimensional hard spheres, *Phys. Rev. E*, **79**, 030201 (2009).

[224] H. Ikeda, F. Zamponi, and A. Ikeda, Mean field theory of the swap Monte Carlo algorithm, *J. Chem. Phys.*, **147**, 234506 (2017).

[225] T. S. Grigera and G. Parisi, Fast Monte Carlo algorithm for supercooled soft spheres, *Phys. Rev. E*, **63**, 045102 (2001).

[226] C. J. Fullerton and L. Berthier, Density controls the kinetic stability of ultra-stable glasses, *Europhys. Lett.*, **119**, 1–7 (2017).

[227] M. Wyart and M. E. Cates, Does a Growing Static Length Scale Control the Glass Transition?, *Phys. Rev. Lett.*, **119**, 1–5 (2017).

[228] E. Vidal Russell and N. E. Israeloff, Direct observation of molecular cooperativity near the glass transition, *Nature*, **408**, 695–698 (2000).

[229] J. C. Conrad, P. P. Dhillon, E. R. Weeks, D. R. Reichman, and D. A. Weitz, Contribution of slow clusters to the bulk elasticity near the colloidal glass transition, *Phys. Rev. Lett.*, **97**, 1–4 (2006).

[230] C. J. O. Reichhardt and C. Reichhardt, Avalanche dynamics for active matter in heterogeneous media, *New J. Phys.*, **20**, 025002 (2018).

[231] S. C. Glotzer, Spatially heterogeneous dynamics in liquids: Insights from simulation, *J. Non. Cryst. Solids*, **274**, 342–355 (2000).

[232] G. Biroli, J. P. Bouchaud, K. Miyazaki, and D. R. Reichman, Inhomogeneous mode-coupling theory and growing dynamic length in supercooled liquids, *Phys. Rev. Lett.*, **97**, 1–4 (2006).